

1 CarbonTracker-CH<sub>4</sub>: An assimilation system for estimating  
2 emissions of atmospheric methane

3  
4 L. Bruhwiler<sup>1</sup>, E. Dlugokencky<sup>1</sup>, K. Masarie<sup>1</sup>, M. Ishizawa<sup>2</sup>, A. Andrews<sup>1</sup>, J. Miller<sup>1</sup>, C.  
5 Sweeney<sup>1</sup>, P. Tans<sup>1</sup>, D. Worthy<sup>4</sup>

6  
7 [1]{NOAA Earth System Research Laboratory, Global Monitoring Division, Boulder  
8 Colorado, USA}

9 [2]{National Institute for Environmental Studies, Center for Global Environmental Research,  
10 Tsukuba, Japan}

11 [4]{Environment Canada, Climate Research Division, Toronto, Ontario, Canada}

12  
13 Correspondence to: L. M. Bruhwiler (lori.bruhwiler@noaa.gov)

14  
15 **Abstract**

16 We describe an assimilation system for atmospheric methane (CH<sub>4</sub>),  
17 CarbonTracker-CH<sub>4</sub>, and demonstrate the diagnostic value of global or zonally  
18 averaged CH<sub>4</sub> abundances for evaluating the results. We show that CarbonTracker-  
19 CH<sub>4</sub> is able to simulate the observed zonal average mole fractions and capture inter-  
20 annual variability in emissions quite well at high northern latitudes (53-90N). In  
21 contrast, CarbonTracker-CH<sub>4</sub> is less successful in the tropics where there are few  
22 observations and therefore misses significant variability and is more influenced by  
23 prior flux estimates. CarbonTracker-CH<sub>4</sub> estimates of total fluxes at high northern  
24 latitudes are about  $81 \pm 7$  Tg CH<sub>4</sub> yr<sup>-1</sup>, about 12 Tg CH<sub>4</sub> yr<sup>-1</sup> (13%) lower than prior  
25 estimates, a result that is consistent with other atmospheric inversions. Emissions  
26 from European wetlands are decreased by 30%, a result consistent with previous  
27 work by Bergamaschi et al. (2005); however, unlike their results, emissions from  
28 wetlands in Boreal Eurasia are increased relative to the prior estimate. Although  
29 CarbonTracker-CH<sub>4</sub> does not estimate an increasing trend in emissions from high

1 northern latitudes for 2000 through 2010, significant inter-annual variability in high  
2 northern latitude fluxes is recovered. Exceptionally warm growing season  
3 temperatures in the Arctic occurred in 2007, a year that was also anomalously wet.  
4 Estimated emissions from natural sources were greater than the decadal average by  
5  $4.4 \pm 3.8 \text{ Tg CH}_4 \text{ yr}^{-1}$  in 2007.

6 CarbonTracker-CH<sub>4</sub> estimates for temperate latitudes are only slightly  
7 increased over prior estimates, but about  $10 \text{ Tg CH}_4 \text{ yr}^{-1}$  is redistributed from Asia to  
8 North America. This difference exceeds the estimated uncertainty for North America  
9 ( $\pm 3.5 \text{ Tg CH}_4 \text{ yr}^{-1}$ ). We used time invariant prior flux estimates, so for the period from  
10 2000 to 2006, when the growth rate of global atmospheric CH<sub>4</sub> was very small, the  
11 assimilation does not produce increases in natural or anthropogenic emissions in  
12 contrast to bottom-up emission datasets. After 2006, when atmospheric CH<sub>4</sub> began  
13 its recent increases, CarbonTracker-CH<sub>4</sub> allocates some of the increases to  
14 anthropogenic emissions at temperate latitudes, and some to tropical wetland  
15 emissions. For temperate North America the prior flux increases by about  $4 \text{ Tg CH}_4$   
16  $\text{yr}^{-1}$  during winter when biogenic emissions are small. Examination of the residuals at  
17 some North American observation sites suggests that increased gas and oil  
18 exploration may play a role since sites near fossil fuel production are particularly hard  
19 for the inversion to fit and the prior flux estimates at these sites are apparently lower  
20 and lower over time than what the atmospheric measurements imply.

21 The tropics are not currently well resolved by CarbonTracker-CH<sub>4</sub> due to  
22 sparse observational coverage and a short assimilation window. However, there is a  
23 small uncertainty reduction and posterior emissions are about 18% higher than prior  
24 estimates. Most of this increase is allocated to tropical South America rather than  
25 being distributed among the global tropics. Our estimates for this source region are  
26 about  $32 \pm 4 \text{ Tg CH}_4 \text{ yr}^{-1}$ , in good agreement with the analysis of Melack et al. (2004)  
27 who obtained  $29 \text{ Tg CH}_4 \text{ yr}^{-1}$  for the most productive region, the Amazon Basin.

## 28 **1 Introduction**

29 Methane (CH<sub>4</sub>) is second in importance to carbon dioxide (CO<sub>2</sub>) among greenhouse  
30 gases with significant anthropogenic sources. It has a radiative forcing of,  $0.5 \pm 0.05$   
31  $\text{Wm}^{-2}$ , about 28% that of non-CO<sub>2</sub> atmospheric constituents in 2010 (Hofmann et al,  
32 2006; updated at <http://www.esrl.noaa.gov/gmd/aggi/>). Over a 100-year time

1 horizon CH<sub>4</sub> is 28 times more efficient per mass as a greenhouse gas than CO<sub>2</sub>  
2 (Myhre et al., 2013).

3 Global emissions of CH<sub>4</sub> are between 500 and 600 Tg CH<sub>4</sub> yr<sup>-1</sup> (Kirschke et al,  
4 2013 and this work) and about 40% of this is due to natural sources, mainly  
5 wetlands. The other 60% of global emissions are due to microbial emissions  
6 associated with rice agriculture, livestock and waste, and fugitive emissions from  
7 fossil fuel production and use (Denman et al., 2007). Global emissions have recently  
8 been approximately in balance with global sinks, mainly chemical destruction by  
9 reaction with OH, but also from oxidation by soil microbes, and atmospheric reactions  
10 with O<sup>1</sup>D and Cl in the stratosphere. The lifetime of CH<sub>4</sub> in the atmosphere is about  
11 10 yr (e.g. Dlugokencky et al., 2003) with CO<sub>2</sub> the eventual product of its oxidation.

12 CH<sub>4</sub> has increased from a preindustrial abundance of 722 ± 4 ppb (Etheridge  
13 et al., 1998 after conversion to the NOAA 2004 CH<sub>4</sub> standard scale (Dlugokencky et  
14 al., 2005)) to current values of about 1800 ppb in 2010 (about 2.5 times), and it is  
15 likely that human activity is responsible for most of this increase. Current levels are  
16 unprecedented over at least the last 800 kyr (Loulerge et al., 2008). NOAA  
17 atmospheric network observations extend back to the 1980s, and show that global  
18 CH<sub>4</sub> increased rapidly through the late 1990s, leveled off during the early 2000s and  
19 have recently begun to increase since 2007 (Rigby et al., 2008; Dlugokencky et al.,  
20 2009). The subject of the causes of the recent increase is the topic of much recent  
21 work (e.g. Bousquet et al., 2011), including this study.

22 An important aspect of atmospheric CH<sub>4</sub> is the sensitivity of natural wetland  
23 emissions to climate change. Emissions from the Arctic, in particular, have the  
24 potential to increase significantly as temperatures rise and the vast stores of soil  
25 carbon thaw (e.g. Schuur et al., 2011; Harden et al., 2012). Schaefer et al. (2010)  
26 pointed out that potential carbon emissions from the Arctic could have important  
27 implications for policies aimed at reducing or stabilizing emissions. This clearly  
28 highlights the importance of maintaining long-term measurements of atmospheric  
29 CH<sub>4</sub> in the Arctic, and in this study we hope to further the case for atmospheric  
30 inverse techniques as a tool to diagnose observed atmospheric records (see  
31 previous studies by Hein et al., 1997; Houweling et al., 1999; Chen and Prinn, 2006;  
32 Bergamaschi et al., 2005; Bousquet et al., 2006; Bergamaschi et al, 2013; Houweling

1 et al., 2013).

2 Atmospheric CH<sub>4</sub> is also influenced by diverse human activities, ranging from  
3 food production (ruminants and rice) to waste (sewage and landfills) to fossil fuel  
4 production (coal, oil and gas). Future increases in population could increase  
5 emissions from agriculture and waste as demand for more food production rises,  
6 while the current boom in shale oil/gas exploitation has focused attention on leakage  
7 from drilling, storage and transport of fossil fuel (e.g. Pétron et al., 2012). An obvious  
8 use of an atmospheric assimilation system is to quantify changes in anthropogenic  
9 emissions and attribute increases at policy relevant spatial scales, something that is  
10 possible only with adequate spatial coverage of observations. In this study we will  
11 discuss the degree to which this is currently possible given the coverage of the  
12 current observational network.

13 The work we present here uses only surface observations rather than  
14 combinations of surface observations and retrievals space-based instruments as  
15 used by Bergamaschi et al. (2013) and Houweling et al. (2014). Our study differs  
16 from that of Bergamaschi et al. (2013) since they used a subset of 30 surface  
17 observations sampling mainly background marine air that existed over the entire  
18 decade, as well as satellite retrievals. In our study we have used most available  
19 surface observations, including those that are sensitive to terrestrial emissions (Table  
20 2). We use the same transport model as Bergamaschi et al. (2013) and Houweling  
21 et al. (2014), however, we use a different assimilation technique and different  
22 strategies for weighting observations and priors. We also include a discussion of  
23 observationally derived quantities that useful evaluation of our results.

24 The next section is a detailed description of our CH<sub>4</sub> assimilation system,  
25 CarbonTracker-CH<sub>4</sub>, followed by a detailed evaluation of its performance. In section  
26 4, we discuss results from CarbonTracker-CH<sub>4</sub> for 2000-2010.

27

## 28 **2 The CarbonTracker Ensemble Data Assimilation System**

29

30 The total emission of CH<sub>4</sub> in time and space may be described by:

$$F(x, y, t) = \lambda_1 F_{\text{natural}}(x, y, t) + \lambda_2 \cdot F_{\text{fossil}}(x, y, t) + \lambda_3 \cdot F_{\text{agriculture/waste}}(x, y, t) + \lambda_4 \cdot F_{\text{fire}}(x, y, t) + \lambda_5 \cdot F_{\text{ocean}}(x, y, t)$$

Where  $\lambda_i$  represents a set of linear scaling factors to be estimated in the assimilation that are applied to the fluxes ( $F$ ) by multiplying prior estimates of  $\text{CH}_4$  fluxes to produce the posterior flux estimates. The prior values of the scaling factors is 1. A total of 121 parameters per week are estimated; 10 terrestrial emission processes for 12 continental regions (corresponding to the Transcom 3 continental regions (Gurney et al., 2000) but with the addition of a tropical African region, see <http://transcom.project.asu.edu> for a map, or Fig. 1), and fluxes from the global ocean. Each weekly assimilation step, emissions for the previous 5 weeks are estimated following the fixed lag Kalman smoother methodology described by Bruhwiler et al., (2005). The terrestrial emissions include fugitive emissions from coal, oil and gas production (estimated as one source); agriculture and waste emissions (rice production, for example); livestock and their waste; and emissions from landfills and wastewater. Natural emissions include contributions from wetlands, termites, uptake in soils and wild animals. The final terrestrial emission category is biomass burning, which is treated as a separate category due to the existence of strong spatial constraints coming from satellite observations of locations of large fires. In general, the spatial distribution of the prior flux estimates is an important constraint on the assimilation. For example, the known location of fossil fuel production from bottom-up emission data sets provides information to the assimilation system on whether a signal measured at a particular observation site could have a fossil fuel component. If production areas change over time and not captured by the prior distribution, then fossil fuels will be underestimated by the inversion.

In this study we estimate emissions for continental scale source regions, and although we rely on the prior spatial distribution of the prior emissions to distribute the emissions, the use of large source regions can lead to aggregation errors as shown by Kaminski et al. (2001). An alternative would be to solve for many more sources, possibly at grid scale. However, without significantly more observational constraints, our solution would be very dependent on not only the prior emissions, but also their assumed spatial and temporal covariance. Ultimately, use of space-

1 based observations might be the preferred solution. At present, significant issues  
2 with space-based emissions still exist, such as quantification of biases that vary with  
3 space and time (e.g. Houweling et al., 2013). On the other hand, as discussed by  
4 Bruhwiler et al. (2011), the global network can constrain certain aspects of the  
5 budgets of greenhouse gases, even with its bias towards background atmospheric  
6 sites.

7 We initialized the assimilation using an equilibrated distribution produced by a  
8 previous TM5 run that was scaled to match observed zonal average CH<sub>4</sub> mixing ratio  
9 for the year 2000. The north-south gradient therefore should represent the observed  
10 atmospheric gradient at the surface. Sensitivity runs using synthetic data (not  
11 shown) suggest that spin-up effects are restricted to within in the first half year of the  
12 assimilation.

13

## 14 **2.1 Ensemble Size and Localization**

15 The ensemble Kalman smoother system used to solve for the scalar  
16 multiplication factors is based on that described by Peters et al. (2005), and uses the  
17 square root ensemble Kalman filter of Whitaker and Hamill (2002). The length of the  
18 smoother window is restricted to five weeks for computational efficiency. Although  
19 the posterior flux estimates in relatively densely sampled regions such as North  
20 America were found to be robust by Peters et al. (2005) with a window this short,  
21 regions with less dense observational coverage (the tropics, for example) are likely to  
22 be poorly constrained even after more than a month of transport and therefore not  
23 well resolved. As pointed out by Bruhwiler et al. (2005), a smoother window of at  
24 least 3 months is likely to make maximal use of remote network sites, however this  
25 may come at the expense of accumulated errors in transport as claimed by Peters et  
26 al. (2007). The extent to which this is true is a subject for further study. Even without  
27 the problem of a short smoother window, the sparseness of the observational  
28 network makes it difficult to resolve under-sampled regions such as the tropical  
29 terrestrial biosphere (Bruhwiler et al., 2011).

30 Statistics for the ensemble are created from 500 members using the prior  
31 covariance matrix of the parameters, each with its own background CH<sub>4</sub>

1 concentration field to represent the time history (and thus covariances) of the filter.  
2 We experimented with different numbers of ensemble members and found that the  
3 use of too few ensemble members results in solutions that stay artificially close to  
4 prior flux estimates. To dampen spurious noise due to the approximation of the  
5 covariance matrix, we apply localization (Houtekamer and Mitchell, 1998) for non-  
6 background sites. By limiting correlations between distant sites, localization ensures  
7 that random correlations between parameters do not translate into unrealistic  
8 constraints on emissions by distant measurement sites (i.e. those connections  
9 physically impossible with only 5 weeks of transport). Following Peters (2005)  
10 localization is based on the linear correlation coefficient between the 500-parameter  
11 deviations and 500 observation deviations for each parameter, with a cut-off at 95%  
12 significance in a student's t-test with a two-tailed probability distribution.

13 As noted above, the posterior covariance matrix is approximated by using the  
14 posterior parameter deviations. Temporal covariance is limited to the period spanned  
15 by the assimilation window. Therefore, time aggregated quantities, such as annual  
16 uncertainties will likely be overestimates since information about temporal  
17 covariations will be limited. Furthermore, as with any inversion, the error covariance  
18 matrix ultimately reflects the relative weighting between the model-data mismatch  
19 errors and prior emission uncertainties that are specified.

## 20 **2.2 Covariance Structure**

21 In our assimilation, the chosen  $1-\sigma$  error of the prior estimates is 75% for all  
22 parameters. The prior covariance structure describes the uncertainty on each  
23 parameter, plus their correlation in space. For the current version of CarbonTracker-  
24 CH<sub>4</sub>, we assumed a diagonal prior covariance matrix so that no prior correlations  
25 between estimated parameters exist. The effect of this choice may be strong anti-  
26 correlations among estimated parameters in regions where few observational  
27 constraints exist; however, larger-scale aggregations of these regions are expected  
28 to yield more robust estimates. For example, the total tropical source can be better  
29 determined than the individual regions between which there can be trade-offs in  
30 emissions from time step to time step. Note also that the 5-week assimilation window  
31 used by CarbonTracker limits knowledge of temporal correlations. As a result, the

1 uncertainty on annual average emissions is difficult to estimate.

## 2 **2.3 TM5 Atmospheric Transport Model**

3

4 Transport Model 5 (TM5, Krol et al, 2005) is a community supported global  
5 model with two-way nested grids. For CarbonTracker-CH<sub>4</sub>, we ran the simulation at  
6 4° latitude x 6° longitude resolution without zoom regions. TM5 is developed and  
7 maintained jointly by the Institute for Marine and Atmospheric Research Utrecht  
8 (IMAU, The Netherlands), the Joint Research Centre (JRC, Italy), the Royal  
9 Netherlands Meteorological Institute (KNMI, The Netherlands), and NOAA ESRL  
10 (USA). TM5 has detailed treatments of advection, convection (deep and shallow),  
11 and vertical diffusion in the planetary boundary layer and free troposphere. The  
12 winds used for transport in TM5 come from the European Center for Medium range  
13 Weather Forecast (ECMWF) operational forecast model. This "parent" model  
14 currently runs with ~25 km horizontal resolution and 60 layers in the vertical prior to  
15 2006 and 91 layers in the vertical from 2006 onwards.

16 The ECMWF meteorological data are preprocessed into coarser grids and are  
17 converted from wind fields to mass conserving horizontal and vertical mass fluxes.  
18 TM5 runs at an external time step of three hours, but due to the symmetrical operator  
19 splitting between advection, diffusion, emissions and loss the effective time step over  
20 which each process is applied is shorter. The vertical resolution of TM5 used with  
21 CarbonTracker-CH<sub>4</sub> is 34 hybrid sigma-pressure levels (from 2006 onwards; 25  
22 levels for 2000-2005), unevenly spaced with more levels near the surface. At the time  
23 the calculations discussed in this study were done, we did not have the ERA-Interim  
24 reanalysis driving meteorology and older reanalyses did not cover the time span we  
25 were interested in. Comparisons of forward simulations suggest that differences  
26 between ERA-I and OD for CH<sub>4</sub> at surface sites is very small, both before and after  
27 the change in the vertical levels. Assimilations run with both data products for  
28 CarbonTracker (CO<sub>2</sub>) produce virtually indistinguishable results in estimated fluxes (  
29 see <http://www.esrl.noaa.gov/gmd/ccgg/carbontracker/>).

30 As noted by Peters et al. (2004), TM5 overestimates the meridional gradient of  
31 SF<sub>6</sub> by about 20%. A systematic comparison of a suite of transport models described



1 by Denning et al. (1999) found that some transport models appear to underestimate  
2 mixing processes, especially near the surface, while others mix emissions more  
3 rapidly throughout the lower atmosphere. They also found that models that  
4 underestimate mixing produce relatively good simulations of marine boundary layer  
5 sites while overestimating concentrations at continental sites. More diffusive models  
6 produced worse marine boundary layer simulations, but did better for continental  
7 sites. TM5 falls into less-diffusive category, but current ongoing development is  
8 aimed at improving the situation. It must be acknowledged that the emissions  
9 estimates in our study may be biased due to inadequate vertical mixing. For  
10 example, more vertical mixing will diffuse emissions throughout a deeper  
11 atmospheric column, and this may result in higher emissions in order to match  
12 observations.

13

#### 14 **2.4 Prior Emission Estimates for Natural Sources**

15

16 The largest natural emissions of methane are from wetlands, defined as  
17 regions that are permanently or seasonally water logged. Wetlands are a broad  
18 category that includes both high-latitude bogs and fens and tropical swamps.  
19 Saturated soils in warm tropical environments tend to produce the most methane.  
20 However, warming Arctic temperatures raise concerns of increasing output from  
21 high-latitude wetlands and future decomposition of carbon currently stored in frozen  
22 Arctic soils (e.g. Schaefer et al., 2011).

23 Methane is rapidly oxidized by methanotrophic bacteria in overlying aerobic  
24 water columns or unsaturated soil, so the water table must be at or near the surface  
25 and the depth of overlying water must be shallow for large emissions to occur.  
26 Wetland plants have adapted to low oxygen environments by having hollow stems to  
27 allow delivery of oxygen and other gases to root systems. These hollow stems also  
28 allow delivery of methane directly to the atmosphere, and along with ebullition  
29 account for most of transport to the atmosphere. Diffusion also occurs but is a  
30 significantly smaller contribution to the atmosphere. (See Barlett and Harris (1993)  
31 for an extensive overview of wetland emissions.) Bottom-up estimates of global

1 emissions from wetlands are about 150-200 Tg CH<sub>4</sub> yr<sup>-1</sup> with most of this occurring in  
2 tropical regions (Melton et al., 2013). Because emissions are sensitive to  
3 temperature and precipitation, they exhibit significant seasonal cycles, especially at  
4 high latitudes, as well as inter-annual variability due to moisture and temperature  
5 variability.

6 Methane emissions from wetlands are difficult to quantify using assimilation  
7 systems for two reasons; their global spatial distribution is difficult to know accurately,  
8 and there is large variability in emission rates over small spatial scales (meters),  
9 which makes extrapolation to large scales difficult. Here we used the prior flux  
10 estimates of Bergamaschi et al. (2005) that are based on the wetland distribution of  
11 Matthews and Fung (1989) and the wetland emission model of Kaplan (2002) that  
12 parameterizes emissions based on moisture, temperature and soil carbon. The  
13 global total of the prior flux estimate is 175 Tg CH<sub>4</sub> yr<sup>-1</sup>.

14 Other natural sources of methane include enteric fermentation in insects  
15 (mainly termites, Sanderson (1996)) and wild ruminants (Houweling et al.,1999).  
16 Prior values for both of these sources (~ 25 Tg CH<sub>4</sub> yr<sup>-1</sup>) are much smaller than the  
17 wetland source. Oxidation of CH<sub>4</sub> in dry soils (~40 Tg CH<sub>4</sub> yr<sup>-1</sup>, Ridgwell et al. (1999))  
18 is a natural sink of CH<sub>4</sub> and is treated as a negative source in the assimilation.

19

## 20 **2.5 Prior Emission Estimates for Fugitive Emissions from Fossil Fuels**

21

22 Methane is the principal component of natural gas, and leaks to the  
23 atmosphere associated with natural gas production and distribution are a  
24 considerable source. Natural gas is associated with oil production and is often flared,  
25 or simply vented to the atmosphere. Together, anthropogenic emissions from oil and  
26 gas production are thought to contribute about 50 Tg CH<sub>4</sub> yr<sup>-1</sup> (~10% of the global  
27 annual methane emissions, EDGAR 3.2FT2000 (European Commission, JRC, 2009).  
28 Methane is also associated with coal deposits and can be released by extracting and  
29 pulverizing coal. It is often vented directly to the atmosphere from mines, and this  
30 source contributes an additional ~20 Tg CH<sub>4</sub> yr<sup>-1</sup> (EDGAR 3.2FT2000 (European  
31 Commission, JRC, 2009). As Asian economies have undergone rapid growth, coal

1 production there has increased by a factor of about two since 2000, while remaining  
2 approximately level for most of the rest of the world. In 2010, production of coal by  
3 China increased by 9% over the previous year (BP Statistical Energy Review, 2011).

4 Combustion of natural gas is currently used to generate about a quarter of the  
5 electricity produced in the U.S. Its popularity as a fuel has recently grown because it  
6 is a relatively clean and efficient source of energy. Recent technological advances in  
7 recovery of natural gas, principally hydraulic fracturing, have led to increases in  
8 reserve estimates, and a tremendous increase in exploitation of shale oil/gas  
9 deposits in North America (e.g. Energy Information Administration;  
10 <http://www.eia.gov>). It is possible that as natural gas reserves are increasingly  
11 exploited, emissions related to its production and distribution will rise in the future.

12 CarbonTracker-CH<sub>4</sub> uses the 1°x1° gridded emissions from EDGAR  
13 3.2FT2000 (European Commission, JRC, (2009) as prior emission estimates for  
14 fugitive emissions from coal, oil and gas production. This data set is based on  
15 emission inventories by country and sector for 1990 and 1995 extrapolated to 2000  
16 using production and consumption statistics. We have not extrapolated this data over  
17 the period covered by CarbonTracker-CH<sub>4</sub>, and have instead kept prior emission  
18 estimates constant at 2000 levels. This will allow us to test whether the emission  
19 estimates suggest changes in anthropogenic emissions, for example, the large  
20 increase in emissions from coal production in Asia or the significant increase in oil  
21 and gas drilling over the last decade in North America. In some cases, the spatial  
22 distributions of priors may not be accurate since they may be based on simple  
23 assumptions like population. For other emissions, there may have been changes in  
24 the spatial distribution of emissions over the decade, oil and gas drilling in North  
25 America for example. The atmospheric inversions allow the possibility of diagnosing  
26 these problems in the underlying prior emission datasets and may lead to  
27 improvements in methodology.

## 28 29 **2.6 Prior Emission Estimates for Agriculture and Waste**

30  
31 The largest source of methane emitted by human activity is agriculture and

1 waste; emissions from rice agriculture, waste/wastewater, and animals and their  
2 waste total 230-250 Tg CH<sub>4</sub> yr<sup>-1</sup>. Ruminants, such as cattle, goats, sheep and water  
3 buffalo are able to convert hard-to-digest forage to energy through enteric  
4 fermentation, in which microbes produce easily digested material inside the animal's  
5 gut. Emissions from enteric fermentation may be expected to increase with  
6 increasing human population and higher standards of living. Animal waste, along with  
7 wastewater and landfills produce CH<sub>4</sub> when conditions favor anaerobic  
8 decomposition. Organic material is decomposed in low oxygen conditions by chains  
9 of microbial processes that terminate in production of methane by methanogens.

10 Rice agriculture is also a significant source of methane to the atmosphere.  
11 This is because warm, waterlogged organic-rich soils in rice paddies are ideal for  
12 methanogenesis. Bottom-up estimates of emissions from rice agriculture are 50 Tg  
13 CH<sub>4</sub> yr<sup>-1</sup>, and emissions can be significantly reduced by drainage of paddies between  
14 harvests as well as other agricultural practices (Yan et al., 2009).

15 CarbonTracker-CH<sub>4</sub> uses the 1°x1° degree gridded emissions from the  
16 EDGAR 3.2FT2000 as prior emission estimates for enteric fermentation, animal  
17 waste management, wastewater and landfills. This data set is based on emission  
18 inventories by country and sector for the years 1990 and 1995 extrapolated to 2000  
19 using production and consumption statistics. For rice agriculture, we used the  
20 seasonally varying emissions of Matthews et al. (1991). We have not extrapolated  
21 this data over the period covered by CarbonTracker-CH<sub>4</sub>, and have instead kept prior  
22 emission estimates constant at 2000 levels as for fossil fuel emissions.

23

## 24 **2.7 Prior Emission Estimates for Biomass Burning**

25

26 Fires are a relatively small part of the atmospheric CH<sub>4</sub> budget: 15-20 Tg CH<sub>4</sub>  
27 yr<sup>-1</sup> out of a total of ~520 Tg CH<sub>4</sub> yr<sup>-1</sup>, however, they are an important contribution to  
28 inter-annual variability of methane.

29 The fire prior currently used in CarbonTracker-CH<sub>4</sub> is based on the Global Fire  
30 Emissions Database (GFED), which uses the CASA biogeochemical model to  
31 estimate the carbon fuel in various biomass pools along with burned area based on

1 MODIS satellite observations of fire counts (Giglio et al., 2006; van der Werf et al.,  
2 2006). The dataset consists of 1°x1° gridded monthly burned area, fuel loads,  
3 combustion completeness, and fire emissions for numerous atmospheric  
4 constituents, including CH<sub>4</sub> for the time period spanning January 1997 - December  
5 2010.

## 6 **2.8 Prior Estimates for Ocean Fluxes**

7  
8 The oceans play a relatively small role in the budget of atmospheric methane,  
9 contributing only ~2-3% of global emissions (~10-15 Tg CH<sub>4</sub> yr<sup>-1</sup>). A significant  
10 fraction of this is assumed to come from methane seeps in shallow coastal waters  
11 (~5 Tg CH<sub>4</sub> yr<sup>-1</sup>). The overlying water column must be shallow for emission to the  
12 atmosphere, since CH<sub>4</sub> is efficiently consumed by aerobic microbial processes. The  
13 water column also needs to be shallow for bubbles to deliver methane directly to the  
14 air. Coastal waters are sometimes supersaturated in CH<sub>4</sub>, and may emit about 6 Tg  
15 CH<sub>4</sub> yr<sup>-1</sup> to the atmosphere, while the open may add another 3 Tg CH<sub>4</sub> yr<sup>-1</sup>  
16 (Houweling et al., 1999; Lambert and Schmidt, 1993).

17 Rhee et al. (2009) have suggested that global ocean emissions excluding  
18 natural seeps is much smaller than the ~9 Tg CH<sub>4</sub> yr<sup>-1</sup> we have used in this version of  
19 CarbonTracker-CH<sub>4</sub>, only about 0.6-1.2 Tg CH<sub>4</sub> yr<sup>-1</sup>. On the other hand, recent  
20 studies conducted in the coastal waters of the eastern Siberian Arctic hint at the  
21 possibility of a significant source of methane coming from methane bubbling from the  
22 continental shelf sediments (Shakova et al., 2010). For this version of  
23 CarbonTracker-CH<sub>4</sub> we followed the approach of Bergamaschi et al. (2009) and used  
24 the estimates of Houweling et al., (1999) and Lambert and Schmidt (1993) as prior  
25 flux estimates. We also assumed an uncertainty on these prior flux estimates of  
26 ±75%.

27

## 28 **2.9 Atmospheric Chemical Loss**

29

30 Methane is removed from the atmosphere mainly by reaction with hydroxyl

1 radical (OH), but also by reaction with atomic chlorine (Cl) and excited-state oxygen  
2 ( $O^1D$ ) in the stratosphere. The chemical loss of methane over a year is about equal  
3 to the total input from sources ( $\sim 520 \text{ Tg CH}_4 \text{ yr}^{-1}$ ), and the mean lifetime of methane  
4 is 9-10 yr. Small differences in the emissions and losses lead to trends in  
5 atmospheric  $\text{CH}_4$  abundance, while year to year changes in the balance of emissions  
6 and loss lead to inter-annual variability and possibly to trends in observed methane.

7 Hydroxyl radical is extremely reactive and has such a short atmospheric  
8 residence time that it is difficult to directly measure its global distribution. Instead,  
9 observations of atmospheric species that have relatively well-quantified  
10 anthropogenic emissions and are destroyed only by reaction with OH, such as methyl  
11 chloroform ( $\text{CH}_3\text{CCl}_3$ ), are used, often along with atmospheric models, to estimate  
12 the abundance of atmospheric OH. Using an empirical approach, Montzka et al.  
13 (2011) noted that the inter-annual variability in atmospheric OH is likely to be within  
14 about  $\sim 2\%$ . Errors in derived OH distributions arise from uncertainty in the emissions  
15 of  $\text{CH}_3\text{CCl}_3$  used to estimate OH and uncertainties in transport models. Krol et al.  
16 (1998) estimated that the uncertainty in globally averaged OH is  $\pm 10\%$ .

17 About 10% of total chemical loss is due to transport and chemical destruction  
18 in the stratosphere. A small amount of this methane-depleted air is returned to the  
19 troposphere and could influence interpretation of high-altitude (aircraft)  
20 measurements of methane. In addition, errors in simulating stratosphere-troposphere  
21 transport could result in biases for model simulations covering many years.

22 Errors in the chemical loss of methane and the inability to adequately resolve  
23 inter-annual variability of OH are troublesome for estimation of methane fluxes. A 2%  
24 variation in the global methane sink is equivalent to  $\sim 10 \text{ Tg CH}_4 \text{ yr}^{-1}$ , about the size of  
25 estimated inter-annual variability in methane emissions.

26 For the present version of CarbonTracker- $\text{CH}_4$  we use pre-calculated OH  
27 fields from a full-chemistry TM5 simulation that have been optimized against global  
28 observations of methyl chloroform. The chemical loss fields consist of a single,  
29 repeating seasonal cycle, and result in a methane lifetime of about 9.5 yr. Details of  
30 the chemical loss fields may be found in Bergamaschi et al. (2005).

## 31 **2.10 Observational Constraints**

1           This study uses measurements of air samples collected at surface sites in the  
2 NOAA ESRL Cooperative Global Air Sampling Network ([http://www.esrl.noaa.gov/  
3 gmd/ccgg/flask.html](http://www.esrl.noaa.gov/gmd/ccgg/flask.html)) except those identified as having analysis or sampling  
4 problems, or those thought to be strongly influenced by local sources. The availability  
5 of data varies over time. Data collection, quality control and analysis methods are  
6 described in detail by Dlugokencky et al. (1994). A map of sites used in  
7 CarbonTracker-CH<sub>4</sub> is shown in Figure 1. In addition, we use in situ quasi-continuous  
8 CH<sub>4</sub> time series from the following towers operated by Environment Canada (EC): 30  
9 m above ground level (agl) at Candle Lake (CDL, formerly Old Black Spruce), SK,  
10 Canada, 105m agl at East Trout Lake, SK, Canada (ETL), 40 m agl at Fraserdale,  
11 ON, Canada (FRD), and 10 m agl at Lac Labiche, AB, Canada (LLB). Other in situ  
12 quasi-continuous CH<sub>4</sub> time series used are from the EC Canadian sites at Alert,  
13 Nunavut (ALT), Sable Island, NS (SBL) and Egbert, ON (EGB). All observations used  
14 in CarbonTracker-CH<sub>4</sub> are calibrated against the WMO GAW CH<sub>4</sub> X2004 mole  
15 fraction scale (Dlugokencky et al., 2005).

16           For most quasi-continuous sampling sites, we construct an afternoon daytime  
17 average mole fraction for each day from the time series, recognizing that our  
18 atmospheric transport model does not always capture the continental nighttime  
19 stability regime while daytime well-mixed conditions are better matched. Table 1  
20 summarizes how data from the different measurement programs are preprocessed  
21 for this study.

22           We further exclude non-marine boundary layer (MBL) observations that are  
23 very poorly forecasted in our framework following the strategy used with  
24 CarbonTracker-CO<sub>2</sub>. We use the so-called model-data mismatch in this process, a  
25 quantity that represents random error ascribed to each observation to account for  
26 measurement and modeling errors at each site. If the observed-minus-forecasted  
27 mole fraction exceeds 3 times the prescribed mismatch, then the observation is not  
28 used at that time-step of the inversion. This can happen when an air sample  
29 influenced by local emissions is not captured well by our 1°x1° fluxes, or when local  
30 meteorological conditions are not captured by our offline transport fields. A complete  
31 list of sites used in CarbonTracker-CH<sub>4</sub> is given in Table 2, along with the model-data

1 mismatch used, the number of points available, the number that were excluded, and  
2 statistics on the posterior fit to each site.

3 Model-data mismatches were determined by assigning each site to a  
4 particular category; marine boundary layer (7.5 ppb), terrestrial (30 ppb), mixed  
5 marine and terrestrial (15 or 25 ppb), tower (25 or 30 ppb) and hard to fit sites (75  
6 ppb). The model-data mismatch values were based on evaluation of forward runs  
7 and experience gained from CarbonTracker (CO<sub>2</sub>, Peters et al., 2005). We forced  
8 the assimilation to closely match remote marine background sites while some sites  
9 were given a very large model-data mismatch because they are likely influenced by  
10 strong local sources. A complete list of sites and their model-data mismatches is  
11 shown in Table 2.

12

### 13 **3. Evaluation of CarbonTracker-CH<sub>4</sub>**

14

15 In this section we discuss the evaluation of CarbonTracker-CH<sub>4</sub> using three  
16 methods: comparison of prior and posterior residuals (difference between simulated  
17 and observed CH<sub>4</sub> concentration), comparisons to profiles measured from aircraft  
18 that were not used in the assimilation, and comparisons to integrated global and  
19 zonal concentration and growth rate.

20

#### 21 **3.1 Residuals**

22

23 The prior and posterior residuals, calculated by subtracting the observed CH<sub>4</sub>  
24 mole fraction at each site constraining the inversion from the simulated prior or  
25 posterior abundances, are shown in Figure 2. The bottom panel shows that the  
26 balance between the prior emissions and the chemical sink leads to an  
27 underestimate of CH<sub>4</sub> relative to observations at all latitudes. By the end of the  
28 simulation, the negative bias of the model using prior fluxes reaches values up to 75  
29 ppb (compared to a global average of ~1790 ppb in 2009, about 4%). This negative  
30 bias is considerably reduced for the posterior residuals, as is shown in the top panel,



1 and at most sites the posterior residuals are within ~15 ppb of the observations. This  
2 is partly by design, since the model-data mismatch determines how closely the  
3 posterior CH<sub>4</sub> abundances must match the observations; however, as Table 1 shows,  
4 the posterior residuals even for some sites that have large model-data mismatch  
5 error assigned to them, can be quite small. An example is BKT, with a model-data  
6 mismatch of 75 ppb and a posterior residual of only 6.8 ppb. For sites like this, future  
7 inversions could use reduced model-data mismatch errors, allowing the observations  
8 to more strongly constrain the inversion.

9 Figure 2 shows that even after assimilation of observations, some sites have  
10 large low biases (implying emissions higher than prior estimates are needed to match  
11 the observations) and Figure 3 shows the relative sizes of the residuals. WGC  
12 (Walnut Grove, CA is located in near a densely populated urban area and agriculture  
13 and has an average posterior residual of -118 ppb. In addition to the difficulty of  
14 using relatively coarse resolution global transport to simulate observations amidst  
15 strong local sources, it is also likely that the prior emissions are underestimated.  
16 Other sites with large biases are WKT (central Texas) and SGP (Southern Great  
17 Plains, OK) with average residuals of -49 ppb and -57 ppb. These sites see transport  
18 from polluted urban areas, and they likely also see transport of emissions from oil  
19 and gas drilling as discussed in more detail below. Some of the Environment  
20 Canada sites also have large negative biases. LLB (Lac Labiche, Canada) for  
21 example, has an average residual of -80 ppb, and it is located close to possible  
22 wetland sources as well as fossil fuel operations.

23

### 24 **3.2 Comparison to Aircraft Profiles**

25

26 The current version of CarbonTracker-CH<sub>4</sub> does not assimilate observations  
27 from the NOAA GMD aircraft project. This network currently consists of 17 sites  
28 distributed over North America where air samples are collected at 12 altitudes and  
29 analyzed for a suite of atmospheric gases, including CH<sub>4</sub>  
30 (<http://www.esrl.noaa.gov/gmd/ccgg/aircraft/>). Because the aircraft observations  
31 were not used to constrain the inversion, these data can be used as an independent

1 check on the inversion. In addition, they provide useful insight into the performance  
2 of TM5's vertical transport.

3 Figure 4 shows the prior and posterior residuals for THD (Trinidad Head, CA),  
4 where the white line represents the average of the residuals and the red lines show  
5 the standard deviation of the residuals as a function of altitude. Compared to the prior  
6 residuals, the posterior residuals show a reduction in bias at all altitudes, as well as a  
7 smaller spread in the residuals. At high altitudes the surface data constraints have  
8 resulted in estimated emissions that are in good agreement with the well-mixed free  
9 tropospheric abundances. THD shows good agreement at the lowest levels because  
10 profiles at this location are more likely to sample background marine air coming off of  
11 the Pacific Ocean. In contrast, the continental site, DND (Dahlen, North Dakota)  
12 shows a much larger negative bias at low altitudes during the summer but good  
13 agreement at all levels during winter (Figure 5). This implies that local or regional-  
14 scale sources that are not included in the CarbonTracker-CH<sub>4</sub> prior and are not  
15 "seen" by other sites influence these summertime profiles. Similar results are found  
16 for other aircraft sites distributed throughout the central U.S. Some sites, however,  
17 show larger biases near the surface. Figure 6 shows both prior and posterior  
18 residuals at TGC (Texas Gulf Coast), a site that sees both continental and marine air,  
19 and also air from nearby industrial and urban centers along the Texas Gulf Coast.  
20 Even after the inversion, the residuals near the surface are still quite large indicating  
21 that the priors and the observations constraining are not able to account for strong  
22 local sources.

23 Figure 7 shows prior and posterior residuals for Poker Flat, Alaska. Note that  
24 even after the inversion, methane abundance is underestimated near the surface.  
25 This is likely the result of underestimation of prior wetland emissions, along with  
26 observational constraints that contain information about interior Alaska. On the other  
27 hand, as we will show below Arctic sites sampling background air likely capture the  
28 large scale methane budget fairly well. Figure 7 demonstrates the importance of  
29 sampling sites near sources for constraining regional methane budgets. Future  
30 versions of CarbonTracker-CH<sub>4</sub> may use at least the lower levels of the aircraft  
31 observations in order to better constrain emissions.

32

### 1 3.3 Global and Zonal Averages

2

3 The abundance of CH<sub>4</sub> integrated over the global atmosphere and its growth  
4 rate are important diagnostics of inversion performance (Rayner et al., 2004;  
5 Bruhwiler et al., 2011; Bergamaschi et al., 2013) because given the ~10 year lifetime  
6 of CH<sub>4</sub>, on global scales emissions and sinks must balance in a way that produces  
7 the observed global growth of CH<sub>4</sub>. Here we follow the approach taken by Bruhwiler  
8 et al. (2011) that uses the same sampling, filtering and smoothing procedure used to  
9 produce the observed global and zonal CH<sub>4</sub> abundances for both data and model  
10 output (see Masarie and Tans (1995) and web updates at [esrl.noaa.gov/gmd](http://esrl.noaa.gov/gmd) for a  
11 description of the data extension procedure). Zonal averages are constructed using  
12 mainly marine boundary layer sites by removing a long term trend approximated as a  
13 quadratic function, deseasonalizing by subtracting an average seasonal cycle, and  
14 using a low-pass digital filter with a half width of 40 days. Importantly, the model is  
15 sampled at the same times as the observations and missing data are filled in the  
16 same way for both the observations and simulations. The simulated and observed  
17 zonal averages are therefore comparable. As shown in the top panel of Figure 8, the  
18 global posterior CH<sub>4</sub> abundance produced by the CarbonTracker-CH<sub>4</sub> assimilation is  
19 in fairly good agreement with the observed global abundance, however it is biased  
20 low by about 10 ppb. This is because the global abundance that results from use of  
21 the prior fluxes without optimization is much lower than observed, and the posterior  
22 global total represents a compromise between CH<sub>4</sub> abundance obtained from prior  
23 flux estimates and the observations at each site. Reducing the model-data mismatch  
24 error and/or increasing the prior flux uncertainty would improve the agreement  
25 between posterior CH<sub>4</sub> and the observations, but likely at the expense of having flux  
26 estimates with unrealistic spatiotemporal variability, especially in regions that are  
27 relatively unconstrained by observations. On the other hand, if the prior flux  
28 estimates are weighted too heavily in the inversion, the posterior global total more  
29 closely follows the global abundance simulated by the prior fluxes than the  
30 observations, and these may depart significantly from the actual emissions. The  
31 middle panel of Figure 8 shows the difference between the simulated and prior CH<sub>4</sub>  
32 abundance and the observations, where it can be seen that the residual difference

1 varies slightly over time as the bias resulting from prior emissions changes. In  
2 particular, between 2004 and 2006, the prior residuals are fairly constant and the  
3 residual between the posterior and the observations is smaller than over other  
4 periods. The conclusions that can be drawn from this are that better prior flux  
5 estimates are needed for future versions of CarbonTracker-CH<sub>4</sub>, and that the global  
6 abundance is a useful way to judge whether the solution is most influenced by the  
7 prior information or by the observational constraints.

8         The bottom panel of Figure 8 shows the growth rate of global atmospheric  
9 CH<sub>4</sub>, a quantity that is directly related to imbalances between emissions and sinks.  
10 CarbonTracker-CH<sub>4</sub> follows the observed growth rate fairly well, but not perfectly  
11 since there are periods for which it under- or overestimates the observed growth rate.  
12 During 2007, for example, the observed growth was underestimated by ~30%, while  
13 during 2009 it was overestimated by about the same amount. These differences are  
14 an indication of global total biases in estimated emissions. The posterior global  
15 growth rate of CH<sub>4</sub> was also computed by Bergamaschi et al. (2013) for their  
16 inversions. They find a maximum growth rate of about 10 ppb yr<sup>-1</sup> for 2007, closer to  
17 the observed growth rate shown in Figure 8 even when the surface observations only  
18 are used in the assimilation. This implies a possible role for the relatively short  
19 assimilation window of CarbonTracker in accounting for the underestimate in global  
20 growth. If the anomalous growth occurs in the tropics and this information cannot  
21 propagate to remote sites due to a short window, variability will be missed. As  
22 discussed by Bruhwiler et al. (2005), an assimilation window of 12 weeks is ideal for  
23 the surface network, but computational issues prevented its use for this study. On  
24 the other hand Figure 8 shows that the anomalous global growth is only slightly  
25 overestimated in 2003, while Bergamaschi et al. (2013) may underestimate this  
26 feature.

27         It is also informative to consider zonally averaged CH<sub>4</sub> mole fraction and its  
28 growth rate at sub-hemispheric scales as shown in Figure 9 for the high northern  
29 latitudes (53.1N-90N), Figure 10 for the tropics (17.5S-17.5N) and Figure 11 for the  
30 southern temperate latitudes (17.5S-53S). For the high northern latitudes, the  
31 posterior simulated integrated CH<sub>4</sub> is quite close to the observations and the growth  
32 rate agrees well with the observed growth rate. On the other hand, the simulated

1 integrated CH<sub>4</sub> in the tropics is further from the observations and closer to the prior  
2 than for the high northern latitudes. The posterior zonal average CH<sub>4</sub> abundance is  
3 closer to the observations for the southern temperate latitude zone, however, the  
4 growth rate differences suggest some interannual variability differences, possibly the  
5 result of transport from tropical latitudes considering the relatively small contribution  
6 these latitudes make to the global methane budget. The simulated growth rate in the  
7 tropics also can differ significantly from the observed growth rate, with under or over  
8 estimates reaching 5 ppb/yr or more. As a comparison, the agreement between the  
9 observed and simulated growth rate at northern polar latitudes is usually well within a  
10 few ppb/yr. The middle panels of Figure 9, 10 and 11 show that when the residuals  
11 between the prior and observations decrease, the posterior residuals are also  
12 smaller.

13 For the high northern latitudes, a small seasonal cycle in the residuals  
14 potentially provides some information about which emission processes may be  
15 under- or overestimated by the priors. Differences between simulated and observed  
16 CH<sub>4</sub> are largest during the winter with the observations being higher than the  
17 simulations. This implies that mid- and high latitude emissions from anthropogenic  
18 sources may be underestimated by the priors and not completely corrected for by the  
19 inversion. Note that biogenic emissions at mid- and high latitudes are at a minimum  
20 during winter.

21 Anomalously high growth rates were observed in 2007 both in the Arctic and  
22 in the tropics (Dlugokencky et al., 2009), a year when the Arctic was anomalously  
23 warm and the tropics were unusually wet. The results shown in Figure 9 suggest that  
24 the inversion is likely able to provide good estimates of flux anomalies in high  
25 latitudes, at least in the zonal average. For the tropics zonal average flux anomaly  
26 estimates for this year are likely to be underestimated. These differences in the  
27 ability of the inversion to recover and attribute variability are due mostly to differences  
28 in the distribution of network sites with the Arctic having better observational  
29 coverage than the tropics. Another factor is that the deep vertical mixing of the  
30 tropical atmosphere makes it difficult for the network sites that are mostly located on  
31 remote islands to detect signals from terrestrial CH<sub>4</sub> sources. A further limitation is

1 the 5-week lag used in CarbonTracker's EnKF scheme that cuts off transport of  
2 signals that are transported to remote observing sites.

3 Note that an additional diagnostic of posterior emissions is the posterior error  
4 covariance and its difference from the prior covariance. If there are no observations  
5 to constrain the posterior estimates, then the posterior error covariance will be  
6 unchanged from the prior error covariance. While the posterior error covariance is a  
7 very useful diagnostic of the error reduction coming from observations, it is less  
8 useful as an indicator of the absolute accuracy of the estimated emissions because  
9 the accuracy of the prior estimates is ultimately not very well known, and there are  
10 transport errors that cannot be adequately accounted for.

11

## 12 **4. Results**

### 13 **4.1 The High Northern Latitudes**

14

15 Here the high northern latitudes are an aggregation of the Transcom 3 regions  
16 Boreal North America, Boreal Eurasia and Europe. This spatial division is somewhat  
17 awkward since some of Europe lies south of what could be considered high northern  
18 latitudes. We divide Europe into a northern section that lies poleward of 47N, and a  
19 southern section that is south of 47N, where this latitude is chosen to roughly  
20 correspond with the southern extents of Boreal North American and Boreal Eurasian  
21 source regions. The prior anthropogenic emissions suggest that  $\sim 34 \text{ Tg CH}_4 \text{ yr}^{-1}$  is  
22 emitted from northern Europe, while  $\sim 15 \text{ Tg CH}_4 \text{ yr}^{-1}$  is emitted from southern  
23 Europe. Emissions from wetlands are much larger in the northern Europe than in the  
24 south.

25 The ten-year average posterior aggregated flux for the high northern latitudes  
26 is  $81 \pm 7 \text{ Tg CH}_4 \text{ yr}^{-1}$ , a decrease of a little over  $12 \text{ Tg CH}_4 \text{ yr}^{-1}$  from the prior  
27 aggregated flux. Note that due to the use of a 5- week assimilation window, the  
28 uncertainty estimate does not include temporal error covariance over timescales  
29 longer than this period and it should therefore be regarded as the best estimate  
30 possible for the long term error covariance given the limitations of the current  
31 assimilation scheme. The inversion suggests that most of this decrease is a

1 reduction in natural wetland emissions (8 Tg CH<sub>4</sub> yr<sup>-1</sup>) with the remaining amount  
2 coming from fugitive fossil fuel emissions, although the portioning between these  
3 sources is strongly influenced by the prior distributions and relative locations of  
4 observation sites. Although the observing network could still be considered sparse at  
5 high northern latitudes, the number of existing sites is sufficient to reduce uncertainty  
6 by over 75% from the prior uncertainty. The total posterior flux ranges from 78 Tg  
7 CH<sub>4</sub> yr<sup>-1</sup> in 2004 to just under 86 Tg CH<sub>4</sub> yr<sup>-1</sup> in 2007 (Figure 12), a year that saw  
8 record warm temperatures throughout much of Boreal North America and Boreal  
9 Eurasia, as well as extremely low sea ice coverage (Stroeve et al., 2008).

10 Annual average methane emissions at high northern latitudes are  
11 approximately evenly divided between fugitive emissions from fossil fuels, agriculture  
12 and waste (coming mostly from Europe) and natural wetlands. As a whole, emissions  
13 from fossil fuel leakage are slightly decreased relative to prior estimates by about 4  
14 Tg CH<sub>4</sub> yr<sup>-1</sup> from 33 Tg CH<sub>4</sub> yr<sup>-1</sup>, a change that is slightly larger than the posterior  
15 estimated uncertainty, 3 Tg CH<sub>4</sub> yr<sup>-1</sup>. Note that ~ 4 Tg CH<sub>4</sub> yr<sup>-1</sup> of the 29 Tg CH<sub>4</sub> yr<sup>-1</sup>  
16 due to fugitive fossil fuel emissions comes from southern Europe. Emissions from  
17 agriculture and waste are unchanged. Annual average wetland emissions over the  
18 high northern latitudes are reduced by 26% from a prior of 31 Tg CH<sub>4</sub> yr<sup>-1</sup> to about 23  
19 Tg CH<sub>4</sub> yr<sup>-1</sup>, a difference that is larger than the average estimated of ~ 5 Tg CH<sub>4</sub> yr<sup>-1</sup>.  
20 This result is in agreement with previous studies (e.g. Chen and Prinn, 2006;  
21 Bergamaschi et al., 2007; Spahni et al., 2011). Our results do not agree with the  
22 emission estimates of Bloom et al. (2010). They find that only 2% of global wetland  
23 emissions come from the high northern latitudes, while we find closer to 10%. On the  
24 other hand our results agree within uncertainties with the estimates of McGuire et al.  
25 (2012) based on flux measurements. They find a source of 25 Tg CH<sub>4</sub> yr<sup>-1</sup> from Arctic  
26 tundra wetlands with uncertainty ranging from 10.7 to 38.7 Tg CH<sub>4</sub> yr<sup>-1</sup>. Applying the  
27 same spatial filter for their Arctic tundra region, CarbonTracker-CH<sub>4</sub> estimates a  
28 somewhat smaller 16 ± 5 Tg CH<sub>4</sub> yr<sup>-1</sup>. The fact that field studies may be biased  
29 towards larger emissions could at least partially account for the lower estimate based  
30 on atmospheric observations. On the other hand, we cannot rule out the possibility  
31 that the TM5 representation of the polar atmosphere is too stable, leading to an  
32 accumulation of methane emissions in the lower atmosphere the inversion will  
33 therefore reduce emissions in order to match observations.

1           The estimated flux anomaly during 2007 is  $4.4 \pm 3.8$  Tg CH<sub>4</sub> with a maximum  
2 summer anomaly of 2.3 Tg CH<sub>4</sub> in July (Figure 13). If the anomaly is calculated by  
3 subtracting the 2000-2006 average annual flux the estimated 2007 anomaly is 5.3 Tg  
4 CH<sub>4</sub>, similar to the result found by Bousquet et al. (2011). The results of Bergamaschi  
5 et al. (2013) also seem to be consistent with these estimates (1.2-3.2 Tg CH<sub>4</sub>). Based  
6 on zonal average analysis of network observations, Dlugokencky et al. (2009)  
7 pointed out that in 2007 the global increase of methane was equal to about a 23 Tg  
8 CH<sub>4</sub> imbalance between emissions and sinks, and that the largest increases in CH<sub>4</sub>  
9 growth occurred in the Arctic (>15 ppb/yr). This does not necessarily imply that the  
10 largest surface flux anomalies occurred at high northern latitudes. Bousquet et al.  
11 (2011) noted that the relatively weak vertical mixing characteristic of polar latitudes  
12 results in a larger response in atmospheric CH<sub>4</sub> mole fractions to anomalous surface  
13 emissions than at tropical latitudes where strong vertical mixing rapidly lofts surface  
14 emissions through a deep atmospheric column. Transport models therefore can play  
15 an important role in helping to untangle surface flux signals from variability in  
16 atmospheric transport processes, although care must be taken to also consider  
17 possible biases in modeled transport.

18           In 2008, the flux anomalies dropped to 2.4 Tg CH<sub>4</sub>, or 3 Tg CH<sub>4</sub> if the anomaly  
19 is calculated by subtracting the average annual flux over 2000-2006, as was done by  
20 Bousquet et al. (2011) who obtained 2 TgCH<sub>4</sub> for their INV1 that is similar to  
21 CarbonTracker-CH<sub>4</sub>, but -3 Tg CH<sub>4</sub> yr<sup>-1</sup> using their higher spatial resolution  
22 variational inversion (INV2). As pointed out by Dlugokencky et al. (2009), both 2007  
23 and 2008 were warm with higher than normal precipitation. Posterior covariance  
24 estimates support the independence of estimates for Boreal North America and  
25 Boreal Eurasia since the covariance between these two regions is small; however, it  
26 is difficult to accurately relate variability in observed temperature and moisture  
27 anomalies with variability in estimated emissions because of the sparseness of the  
28 surface observation sites.

29           For the high northern latitudes CarbonTracker-CH<sub>4</sub> is able to distinguish  
30 between different CH<sub>4</sub> source processes and regions. Wetlands may be  
31 distinguished from anthropogenic sources because of the spatial separation of prior  
32 flux constraints; many high northern latitude wetland complexes are located in



1 relatively sparsely populated areas, while fossil fuel and agricultural and waste  
2 emissions are distributed mainly in populated areas of Europe (although the Western  
3 Siberian Lowlands is also a region of intensive fossil fuel production). Ocean  
4 methane fluxes are thought to be small compared to terrestrial fluxes, and northern  
5 Eurasia and boreal North America are separated by the North Pacific Ocean.  
6 Furthermore, the stronger zonal and weaker vertical transport characteristic of the  
7 high latitudes helps to transport flux information to network sites. Both Europe and  
8 boreal North America are at least partially constrained by surface network sites, and  
9 although boreal Eurasia is not adequately covered by network sites, a number of  
10 sites exist downwind of it (Shemya, Barrow and Cold Bay). For Europe, average  
11 trajectory calculations suggest that a large region of wetlands in eastern Scandinavia  
12 and northwestern Russia is constrained by Pallas, Finland. Other sites help to  
13 constrain the anthropogenic sources from the rest of Europe.

14 For boreal North America, prior flux emissions from fossil fuels and agriculture  
15 and waste form an insignificant part of total methane emissions. This is not the case  
16 for Europe for which emissions are more evenly divided between anthropogenic and  
17 wetland emissions. Note that about 40% of the agricultural emissions and 22% of  
18 the fossil fuel emissions are from southern Europe. Prior emission estimates from  
19 natural sources for Europe, the majority of which lie in northern Europe, are about 45  
20 Tg CH<sub>4</sub> yr<sup>-1</sup> during the summer months while the 11-year average posterior summer  
21 estimate is about 13 Tg CH<sub>4</sub> yr<sup>-1</sup>, a large reduction. The uncertainty estimates,  
22 however, only decrease by at most 15% implying that the sources categories are not  
23 strongly constrained by observations. Boreal Eurasian summertime wetland emissions  
24 are increased relative to the prior flux estimates from 26 Tg CH<sub>4</sub> yr<sup>-1</sup> to 37 Tg CH<sub>4</sub> yr<sup>-1</sup>,  
25 and posterior uncertainties decrease from prior uncertainties by ~20-25%. For  
26 boreal North America, the average posterior summer wetland flux is only slightly  
27 below the prior flux estimate (about 19 Tg CH<sub>4</sub> yr<sup>-1</sup> compared to about 16 Tg CH<sub>4</sub> yr<sup>-1</sup>,  
28 a difference that is within the summer average posterior estimated uncertainty of ~10  
29 Tg CH<sub>4</sub> yr<sup>-1</sup>). The redistribution of emissions from Europe to northern Eurasia was  
30 found by Chen and Prinn (2006) to be sensitive to the choice of sites used in the  
31 inversion, however, our results indicate that the observations imply that while prior  
32 emissions are too high for Europe, larger emissions are still needed elsewhere to  
33 match the meridional distribution of observed methane. Bergamaschi et al. (2005)

1 also found decreased emissions for Europe relative to prior estimates, but  
2 interestingly, their inversion also reduced high-latitude emissions from prior estimates  
3 for other high latitude source regions as well. During the winter months, when  
4 biogenic emissions are low, prior estimates are decreased by the inversion for both  
5 Boreal Eurasia (-20%) and Europe (-8%) and relatively unchanged for boreal North  
6 America. The small change in winter European emissions supports the conclusion  
7 that prior wetland emissions for Europe are indeed overestimated. Note that prior  
8 emissions for wetland emissions from northern Europe are about equal to fugitive  
9 emissions from fossil fuels.

10 High latitude emissions of CH<sub>4</sub> from agriculture and waste are significant only  
11 for Europe, and estimated fluxes are unchanged from prior estimates. Fugitive  
12 emissions of CH<sub>4</sub> from fossil fuel production are reduced from prior estimates for  
13 Europe and boreal Eurasia by 2 Tg CH<sub>4</sub> yr<sup>-1</sup> for each region; from 21 ± 4 Tg CH<sub>4</sub> yr<sup>-1</sup>  
14 and 12 ± 2 Tg CH<sub>4</sub> yr<sup>-1</sup>. Reductions in uncertainty are fairly large for Europe, ~35%,  
15 and about ~32% for Boreal Eurasia. For boreal North America, prior estimates of  
16 fossil fuel emissions of CH<sub>4</sub> are very small (< 1 Tg CH<sub>4</sub> yr<sup>-1</sup>), and it should be noted  
17 that the tar sand production areas are in the temperate North American TransCom 3  
18 source region rather than Boreal North America.

19 Significant natural CH<sub>4</sub> emissions have recently been proposed for the high  
20 northern latitudes. Walter et al., (2007) estimated that in addition to emissions from  
21 High Northern Latitude wetlands (31 Tg CH<sub>4</sub> yr<sup>-1</sup> for the CarbonTracker-CH<sub>4</sub> prior),  
22 ebullition from arctic lakes could add an additional 24 ± 10 Tg CH<sub>4</sub> yr<sup>-1</sup>. In addition to  
23 organic rich sediments and subsea permafrost, CH<sub>4</sub> is stored in ice hydrates forming  
24 at the low temperatures and high pressures in sediments at the bottom of the Arctic  
25 Ocean and subsea permafrost, and below terrestrial permafrost as well. Relatively  
26 shallow waters make it possible for bubbles to transport methane directly and rapidly  
27 to the atmosphere. The estimates of Shakhova et al. (2013) estimate the size of the  
28 source from subsea permafrost from the East Siberian shelf alone to be ~17 Tg CH<sub>4</sub>  
29 yr<sup>-1</sup>, although observational records are currently insufficient to establish whether  
30 these emissions are changing over time. Walter et al. (2012) have proposed that a  
31 similar process may also occur on land as permafrost thaws and glaciers melt. Total  
32 natural emissions including all of these processes approaches 65 Tg CH<sub>4</sub> yr<sup>-1</sup>, an

1 amount that significantly exceeds both the average prior and posterior annual natural  
2 emissions for CarbonTracker-CH<sub>4</sub> (31 and 23 Tg CH<sub>4</sub> yr<sup>-1</sup>). Since the average total  
3 posterior CarbonTracker-CH<sub>4</sub> high northern latitude emissions is ~81 Tg CH<sub>4</sub> yr<sup>-1</sup>,  
4 accommodation of a 65 Tg CH<sub>4</sub> yr<sup>-1</sup> natural source would have to come at the  
5 expense of fossil fuel and agriculture/waste sources (average total CarbonTracker-  
6 CH<sub>4</sub> posterior of ~57 Tg CH<sub>4</sub> yr<sup>-1</sup>, with about 12 Tg CH<sub>4</sub> yr<sup>-1</sup> emitted from southern  
7 Europe), which would need to be reduced by about 75%.

8         The estimated mass of carbon thought to be frozen in Arctic permafrost down  
9 to 20 m is estimated to be ~1700 Pg C (Pg = 10<sup>15</sup> g) (Tarnocai et al., 2009),  
10 significantly more carbon than is currently in the atmosphere (~830 Pg C) and over 3  
11 times what has already been emitted to the atmosphere from fossil fuel use since  
12 pre-industrial times. As the Arctic warms and permafrost thaws, this ancient carbon  
13 may be mobilized to the atmosphere and a small fraction (~3%) may be emitted as  
14 CH<sub>4</sub> (Schuur et al., 2011). Recent studies suggest that permafrost carbon will begin  
15 to enter the atmosphere during this century (e.g. Schaefer et al., 2010; Harden et al.,  
16 2012; Melton et al., 2013; Frolking et al., 2011). Harden et al. (2012) predict that 215-  
17 380 PgC will thaw by 2100. Their assessment of the carbon balance of Arctic tundra  
18 based on flux observations McGuire et al. (2012) found that between the 1990s and  
19 2000s emissions of CH<sub>4</sub> doubled (from 13 to 26 Tg CH<sub>4</sub> yr<sup>-1</sup>), results that are  
20 consistent with warmer temperature and longer growing seasons.

21         Detection of trends in Arctic greenhouse gas emissions is difficult using  
22 atmospheric concentration measurements alone because changes are expected to  
23 be small in comparison to transport of much larger mid-latitude emissions. Forward  
24 and inverse modeling techniques can be helpful because they provide the ability to  
25 untangle variability coming from transport from signals associated with local sources.  
26 As shown in Figure 13, posterior CarbonTracker-CH<sub>4</sub> emissions do not indicate that  
27 there has been a trend in natural high northern latitude emissions over the last  
28 decade, although we see strong evidence for substantial inter-annual variability.

29

## 30 **4.2 The Northern Hemisphere Mid-Latitudes**

31

1 For this study, the northern mid-latitudes are composed of the temperate  
2 Eurasia and temperate North America Transcom 3 regions (see Figure 1). The  
3 average estimated total emissions for the northern mid-latitudes over the period  
4 2000-2010 are greater than prior estimates by about 5 Tg CH<sub>4</sub> yr<sup>-1</sup>, increasing from  
5 about 156 ± 27 Tg CH<sub>4</sub> yr<sup>-1</sup> to 162 ± 16 Tg CH<sub>4</sub> yr<sup>-1</sup>. After the tropics, the Northern  
6 Hemisphere mid-latitudes emit the most atmospheric CH<sub>4</sub>. The largest mid-latitude  
7 source of CH<sub>4</sub> is agriculture and waste, and this source rises from 117 ± 26 Tg CH<sub>4</sub>  
8 yr<sup>-1</sup> to 119 ± 15 Tg CH<sub>4</sub> yr<sup>-1</sup>. Natural wetlands are a fairly small contribution to  
9 northern mid-latitude emissions, and they are increased from about 9 ± 3 to 12 ± 2 Tg  
10 CH<sub>4</sub> yr<sup>-1</sup>. For the northern mid-latitudes as a whole, estimated fossil fuel emissions  
11 remain very close to prior estimates at about 31 ± 3 TgCH<sub>4</sub>.

12 In general, CarbonTracker-CH<sub>4</sub> re-distributes prior estimated emissions from  
13 temperate Eurasia to North America (Figure 14). The total prior flux estimates for  
14 temperate Eurasia and temperate North America are 124 ± 22 and 32 ± 5 Tg CH<sub>4</sub> yr<sup>-1</sup>,  
15 respectively. The average posterior estimates are 114 ± 15 and 47 ± 3 Tg CH<sub>4</sub> yr<sup>-1</sup>.  
16 Agriculture and waste emissions from temperate Eurasia are reduced by almost 10  
17 Tg CH<sub>4</sub> yr<sup>-1</sup> (~9%). Fugitive fossil fuel emissions for temperate North America  
18 increase by ~9% (6.7 ± 1.5 to 8 ± 1 Tg CH<sub>4</sub> yr<sup>-1</sup>), agriculture and waste emission  
19 increase by 53% (21 ± 4 to 32 ± 3 Tg CH<sub>4</sub> yr<sup>-1</sup>), and natural emissions increase by  
20 66% (4.5 ± 1 Tg CH<sub>4</sub> yr<sup>-1</sup> to 7.5 ± 1 Tg CH<sub>4</sub> yr<sup>-1</sup>). Posterior uncertainties for both  
21 regions decrease from prior uncertainty by about 30%.

22 In this version of CarbonTracker-CH<sub>4</sub>, we used constant anthropogenic  
23 emissions representative of the year 2000 from the EDGAR v3.2 FT database as  
24 priors. A more recent version of EDGAR (version 4.2, (European Commission, JRC,  
25 2009) reports that global anthropogenic emissions of methane significantly increased  
26 over the last decade, from 309 Tg CH<sub>4</sub> yr<sup>-1</sup> in 2000 to 364 Tg CH<sub>4</sub> yr<sup>-1</sup> by 2008 (an  
27 increase of about 18%). Most of this increase (37 Tg CH<sub>4</sub> yr<sup>-1</sup>) is estimated to have  
28 occurred between 2000 and 2006 according to EDGAR. As we show in Figure 8, the  
29 observed global total CH<sub>4</sub> does not change much between 2000 and 2005. Bousquet  
30 et al. (2006) proposed that increased anthropogenic emissions were balanced by  
31 decreases in wetland emissions for the early 2000s. CarbonTracker-CH<sub>4</sub> is  
32 constrained using a time-invariant prior, and because it must follow the observed

1 global growth rate that flat at least until 2006, it does not find trends in either total  
2 anthropogenic or natural emissions.

3 After 2006 the observed global annual mean CH<sub>4</sub> abundance increased ~25  
4 ppb by 2010, equivalent to additional emissions of ~70 TgCH<sub>4</sub> over 4 years (18 Tg  
5 CH<sub>4</sub> yr<sup>-1</sup>) if mixed uniformly throughout the atmosphere. As discussed in section 3.3,  
6 CarbonTracker-CH<sub>4</sub> follows the global growth rate closely. The average total  
7 emissions from 2000 to 2006 are ~514 ± 22 TgCH<sub>4</sub>, but after 2006 it is 530 ± 22 Tg  
8 CH<sub>4</sub> yr<sup>-1</sup>, an amount that is in approximate agreement with the change in total  
9 emissions implied by observations. CarbonTracker-CH<sub>4</sub> allocates much of this  
10 increase to anthropogenic sources. Average global total anthropogenic emissions are  
11 316 ± 18 Tg CH<sub>4</sub> yr<sup>-1</sup> for 2000 to 2005, increasing to 325 ± 18 Tg CH<sub>4</sub> yr<sup>-1</sup> for 2006 to  
12 2010, a number that is roughly consistent with the constant anthropogenic prior  
13 inversions of Bergamaschi et al. (2013). For the period 2000 to 2005, the estimated  
14 total natural emissions are 198 ± 12 Tg CH<sub>4</sub> yr<sup>-1</sup>, increasing to 204 ± 12 Tg CH<sub>4</sub> yr<sup>-1</sup>  
15 from 2006 to 2010. CarbonTracker-CH<sub>4</sub> assigns the post-2005 estimated increases in  
16 anthropogenic emissions to the populated northern temperate latitudes, while the  
17 bulk of the global increase in natural emissions is assigned to the tropics.

18 The EDGAR emission data imply that anthropogenic emissions of CH<sub>4</sub> grew  
19 rapidly over the last decade, with significant growth occurring between 2000 and  
20 2005, a time when the observed growth rate does not support an upward trend in  
21 emissions. Could decreased emissions from wetlands have cancelled out this  
22 increase as Bousquet *et al.* proposed? More recent work by Bergamaschi et al.  
23 (2013) suggests a large role for anthropogenic emissions, while Houweling et al.  
24 (2013) find that a mixture of anthropogenic and tropical wetland sources are  
25 responsible for the increase since 2006. Although the sparseness of the  
26 observational network makes it impossible to rule this scenario out, the observations  
27 and the spatial constraint they supply to the inversion do not suggest that there was a  
28 trend in wetland emissions over the first half of the decade, although there certainly  
29 was inter-annual variability. On the other hand, this result cannot be reconciled with  
30 bottom-up estimates of increasing anthropogenic emissions over this period. From  
31 2006 through 2010, estimated emissions increased by ~15 Tg CH<sub>4</sub> yr<sup>-1</sup>, slightly less  
32 than the 18 Tg CH<sub>4</sub> yr<sup>-1</sup> estimated by EDGAR for this period, and with considerable

1 inter-annual variability. CarbonTracker-CH<sub>4</sub> divides this growth between  
2 anthropogenic and natural emissions in proportion to their contribution to the prior  
3 global atmospheric CH<sub>4</sub> budget (~60% anthropogenic and ~40% natural). Although it  
4 is likely that both anthropogenic and natural emissions have been increasing since  
5 2006, this latter fact may also be interpreted as evidence of the inability of the  
6 observational network to discriminate between these categories of sources due to  
7 insufficient spatial coverage at lower latitudes. It is possible that the use of observed  
8 isotopic composition of CH<sub>4</sub> could help to distinguish different sources (e.g. Miller et  
9 al., 2002). Uncertainty reductions are substantial for the global totals of both natural  
10 and anthropogenic emissions, ~66% each, and this suggests that observational  
11 constraints are consistent with the prior allocation of emissions between natural and  
12 anthropogenic processes, but does not rule out the possibility that the network  
13 cannot discriminate between the two. Bergamaschi et al. (2013) have also  
14 suggested that the increases in anthropogenic emissions from EDGAR are likely too  
15 high, especially estimates of emissions from Chinese coal production.

16 Anthropogenic emissions from Asia are thought to have been increasing  
17 steeply in recent years. EDGAR v4.2 emissions dataset estimates that total  
18 anthropogenic emissions from China increased from about 50 Tg CH<sub>4</sub> yr<sup>-1</sup> in 2000 to  
19 over 73 Tg CH<sub>4</sub> yr<sup>-1</sup> in 2008, an increase of almost 50%. CarbonTracker-CH<sub>4</sub> does  
20 not show a steady upward trend in emissions from temperate Asia, but there is a 5  
21 Tg CH<sub>4</sub> yr<sup>-1</sup> increase between the average of the first and last five years, a change  
22 that is well within the estimated uncertainty for this region of 15 Tg CH<sub>4</sub> yr<sup>-1</sup>. This is  
23 consistent with the ~5 Tg CH<sub>4</sub> yr<sup>-1</sup> increase in anthropogenic emissions from China  
24 between 2003 and 2008 found by Bergamaschi et al. (2013). For temperate North  
25 America, there does not appear to be much change over the decade in total  
26 estimated emissions; however, fugitive emissions from fossil fuel production in  
27 temperate North America show significant increases from prior emissions during  
28 winter months, when biogenic emissions are smallest (Figure 15). By the end of the  
29 decade, winter fossil fuel emissions from temperate North America end up higher  
30 than prior flux estimates by about 4 Tg CH<sub>4</sub> yr<sup>-1</sup>, exceeding the estimated uncertainty  
31 of ~3 Tg CH<sub>4</sub> yr<sup>-1</sup>. Due to large variability of biogenic emissions, it is difficult to see  
32 evidence of this change during the warmer seasons, and the variability also may  
33 mask evidence of increasing fossil fuel emissions in the total estimated emissions. It

1 is interesting to note that, as shown in Table 1, many of the sites with the largest  
2 residuals are located near potential sources of fugitive emissions from fossil fuel use.  
3 An example is SGP (Southern Great Plains) located in northern Oklahoma. Figure 16  
4 shows that it is increasingly difficult over time for the inversion to fit this site, possibly  
5 due to increasing emissions from fossil fuel production nearby and in northern Texas.  
6 This feature is qualitatively consistent with the results of Miller *et al.* (2013), who  
7 calculated larger than predicted emissions of CH<sub>4</sub> related to fossil fuel extraction in  
8 this part of the USA, although they also acknowledge a possible role for emissions  
9 from livestock. The recent expansion of oil and gas production is not included in the  
10 prior used for CarbonTracker-CH<sub>4</sub>, and the more recent EDGAR4.2 emission product  
11 has more emissions in North America than the prior we used here. Petron *et al.*  
12 (2012) have recently suggested that leakage from fossil fuel production in Colorado's  
13 Denver-Julesburg Basin may be several times larger than estimated by state and  
14 local inventories. Karion *et al.* (2013) have recently shown that emissions from a gas  
15 field in Utah may be much higher than previous estimates as well.

16

### 17 **4.3 The Tropics**

18

19 Tropical emissions are difficult to constrain because of the sparse distribution  
20 of atmospheric observations, but also due to the tendency of the tropical atmosphere  
21 to rapidly mix surface signals throughout a deep atmospheric column. Many of the  
22 observation sites in tropical latitudes are located on islands where they sample  
23 marine air from higher latitudes. Ascension Island, for example often sees air from  
24 the South Atlantic, rather than air transported westward from tropical Africa.  
25 Although the site located in the Seychelles site sometimes sees air from southern  
26 Asia, often it sees air transported from the southern Indian Ocean. In particular, it is  
27 difficult to see how the current observational network can independently constrain  
28 tropical Asia and tropical Africa. On the other hand, Pacific Ocean sites may make it  
29 possible to discriminate between tropical America and Asia.

30 In agreement with the results found by other studies (e.g. Houweling *et al.*,  
31 1999; Bergamaschi *et al.*, 2007; Mikaloff–Fletcher *et al.*, 2004a,b, Houweling *et al.*,  
32 2013), CarbonTracker-CH<sub>4</sub> increases tropical emissions relative to prior estimates.

1 The average total prior emission is  $132 \pm 18 \text{ Tg CH}_4 \text{ yr}^{-1}$  and the posterior total is  
2 about  $157 \pm 11 \text{ Tg CH}_4 \text{ yr}^{-1}$ , an increase of 19%. The estimated uncertainty is  $\pm 11 \text{ Tg}$   
3  $\text{CH}_4 \text{ yr}^{-1}$ , a decrease from the prior uncertainty of about 39%. This suggests that the  
4 observations are able to add some information about tropical emissions to the  
5 inversion. Most of the adjustment in emissions goes to wetlands (an increase of 31%  
6 from  $\sim 65 \text{ Tg CH}_4 \text{ yr}^{-1}$  to  $\sim 84 \text{ Tg CH}_4 \text{ yr}^{-1}$ , with a decrease in uncertainty from 14 to 8  
7  $\text{Tg CH}_4 \text{ yr}^{-1}$ , or 57%). Posterior anthropogenic emissions are essentially unchanged  
8 from priors with posterior emissions of  $49 \text{ Tg CH}_4 \text{ yr}^{-1}$  for agriculture and waste, and  
9  $\sim 7.5 \text{ Tg CH}_4 \text{ yr}^{-1}$  for fossil fuel emissions, with the uncertainty in total anthropogenic  
10 emissions decreasing from  $11 \text{ Tg CH}_4 \text{ yr}^{-1}$  to about  $7 \text{ Tg CH}_4 \text{ yr}^{-1}$ . CASA-GFED prior  
11 flux estimates for biomass burning are increased from about  $10 \text{ Tg CH}_4 \text{ yr}^{-1}$  to  $11 \text{ Tg}$   
12  $\text{CH}_4 \text{ yr}^{-1}$ .

13 Interestingly, the estimated increases in decadal-average emission from  
14 tropical wetlands are not evenly distributed among the tropical regions of South  
15 America, Africa and Asia. Changes are largest for South America, increasing from a  
16 prior of about  $19 \pm 4 \text{ Tg CH}_4 \text{ yr}^{-1}$  to almost  $32 \pm 4 \text{ Tg CH}_4 \text{ yr}^{-1}$  (+68%). For Africa,  
17 posterior emissions increase from  $17 \pm 4 \text{ Tg CH}_4 \text{ yr}^{-1}$  to  $21 \pm 4 \text{ Tg CH}_4 \text{ yr}^{-1}$  (+24%)  
18 and for Asia,  $29 \pm 6 \text{ Tg CH}_4 \text{ yr}^{-1}$  to  $35 \pm 6 \text{ Tg CH}_4 \text{ yr}^{-1}$  (+21%). The estimates from  
19 CarbonTracker-CH<sub>4</sub> compare well with Melack et al. (2004), who estimate that the  
20 Amazon basin emits about  $29 \text{ Tg CH}_4 \text{ yr}^{-1}$  using a combination of field studies and  
21 satellite observations of wetland extent. Estimated emissions from anthropogenic  
22 sources remain very close to prior estimates for all tropical regions, and this is also  
23 the case for biomass burning. For all tropical regions, the posterior uncertainty is  
24 only slightly reduced with respect to the prior uncertainty, generally less than 15%,  
25 and the high posterior correlations between these regions make it difficult to have  
26 confidence that the inversion is able to constrain information about these regions.

27 Although observations indicate inter-annual variability in the CH<sub>4</sub> growth rate in  
28 the tropical marine boundary layer, CarbonTracker-CH<sub>4</sub> is not able to capture this  
29 very well as discussed in the previous section on evaluation. Figure 17 shows both  
30 the increase in posterior CH<sub>4</sub> emission estimates from the prior, as well the inter-  
31 annual variability of the estimates. Total biogenic emissions (e.g. agriculture/waste  
32 and wetlands) were larger than normal during 2007 and 2008 in agreement with the



1 analysis of Dlugokencky et al. (2009), who noted that both of these years were  
2 relatively wet in the tropics. Wet years are also years with lower fire emissions and  
3 the posterior emissions of CarbonTracker-CH<sub>4</sub> show a significant anti-correlation of  
4 fire and wetland emissions as shown in Figure 18, although the estimated  
5 uncertainties on the emission anomalies are quite large.

6 Increases in tropical emissions for 2007 and 2008 are also found by  
7 Bergamaschi et al. (2013) although they show interesting differences between their  
8 inversions that used space-based observations and those using only surface  
9 observations. Houweling et al. (2013) showed that use of space-based observations  
10 with a bias correction that is fixed using independent data rather than estimated by  
11 the inversion results in a re-distribution of emissions from the extra-tropical Northern  
12 Hemisphere to the tropics by ~50 Tg CH<sub>4</sub> yr<sup>-1</sup>. Their tropical emissions over 2003 to  
13 2010 range from 380 to 450 Tg CH<sub>4</sub> yr<sup>-1</sup>, much higher than the values obtained by  
14 this study, although the latitude range of their tropics is not clear. CarbonTracker-CH<sub>4</sub>  
15 values are similar to Houweling et al. (2013) if we use 30S-30N as the latitude range  
16 of the tropics. In addition, Houweling et al. (2013) note that they estimate larger  
17 inter-annual variability in tropical emissions of CH<sub>4</sub> using their preferred bias  
18 correction methodology. Although this may indicate that the space-based  
19 observations are adding significant new information to the inversion, as noted by  
20 Houweling et al. (2013), degradation of the instrument occurred after 2005.

21 In addition to a greatly needed expansion of sites sensitive to the tropical  
22 biosphere [e.g. Miller *et al.*, 2007], progress on constraining tropical emissions could  
23 be made by increasing the length of the assimilation window, allowing signals to  
24 reach existing observation sites from terrestrial tropical source regions, and by using  
25 aircraft observations as constraints in the assimilation. Also since CarbonTracker-  
26 CH<sub>4</sub> seems to miss tropical variability in emissions, it is likely that the growth in global  
27 CH<sub>4</sub> abundance due to tropical wetlands is be greater than the posterior estimates  
28 suggest. Comparisons of posterior CH<sub>4</sub> profiles with profiles measured aircraft at  
29 two sites in Brazil (Fortaleza on the coast, and Santarem in the interior) support both  
30 the underestimate of emissions in the priors and the lack of data to revise the priors  
31 adequately. This was pointed out also by Beck et al. (2012).

1            Since setting up and maintaining observation sites in tropical land regions is  
2 logistically difficult, coverage may never be adequate in these regions. The hope is  
3 that remote sensing observations could provide additional observational constraints,  
4 however, the issue of how to identify and quantify biases in remotely sensed CH<sub>4</sub>  
5 that are be spatially and temporally coherent is still be an important limitation  
6 (Houweling et al., 2013).

#### 8 **4.4 The Southern Hemisphere Mid-Latitudes**

9  
10            Decadal mean CH<sub>4</sub> emission estimates from southern temperate latitudes  
11 (Temperate South America, South Africa and Australia) increase from a prior of 78  
12 Tg CH<sub>4</sub> yr<sup>-1</sup> to 91 Tg CH<sub>4</sub> yr<sup>-1</sup>, an increase of about 17%. The aggregated uncertainty  
13 estimate decreases from about 12 Tg CH<sub>4</sub> yr<sup>-1</sup> to 7 Tg CH<sub>4</sub> yr<sup>-1</sup>, a decrease of about  
14 40%. The largest estimated CH<sub>4</sub> emissions are from temperate South America (54 ±  
15 6 Tg CH<sub>4</sub> yr<sup>-1</sup>), followed by temperate South Africa (22 ± 2 Tg CH<sub>4</sub> yr<sup>-1</sup>) and  
16 Australia/New Zealand (15 ± 2 Tg CH<sub>4</sub> yr<sup>-1</sup>). Annual average flux estimates for the  
17 aggregated total emissions, as well as the individual processes are little changed  
18 from prior estimates for both temperate southern Africa and Australia/New Zealand.  
19 The posterior uncertainty estimates for these regions are essentially unchanged as  
20 well, indicating a lack of significant observational constraints for these regions.

21            On the other hand, aggregated total emissions for temperate South America  
22 are adjusted from 43 ± 7 Tg CH<sub>4</sub> yr<sup>-1</sup> to 54 ± 6 Tg CH<sub>4</sub> yr<sup>-1</sup>, although with a relatively  
23 small uncertainty reduction of about 9%. The adjustment to CH<sub>4</sub> emissions occurs as  
24 an increase from natural biogenic sources, since fossil fuel emissions and  
25 agriculture/waste prior flux estimates are small for this region. Emissions from natural  
26 wetlands increase by 7 Tg CH<sub>4</sub> yr<sup>-1</sup> over prior estimates, and agriculture and waste  
27 by close to 4 Tg CH<sub>4</sub> yr<sup>-1</sup>. The uncertainty reduction for natural wetlands is very  
28 small, while uncertainty estimates for agriculture and waste are about 13% smaller  
29 than the priors.

#### 31 **4.5 The Global Ocean**

1

2 Emissions of CH<sub>4</sub> from oceans are thought to make only a small contribution  
3 to the atmospheric CH<sub>4</sub> budget, with a prior flux estimate in CarbonTracker-CH<sub>4</sub> of  
4 ~15 ± 13Tg CH<sub>4</sub> yr<sup>-1</sup>. Posterior estimates are adjusted downwards to 12.6 Tg CH<sub>4</sub> yr<sup>-1</sup>,  
5 a difference that exceeds the posterior uncertainty estimate of about 15 Tg CH<sub>4</sub> yr<sup>-1</sup>.  
6 Rhee et al. (2009) have proposed that earlier estimates of the oceanic methane  
7 emissions were biased towards supersaturated waters, and that the emissions are  
8 much lower, about 0.6-1.2 Tg CH<sub>4</sub> yr<sup>-1</sup>, a decrease of over a factor of 10. It is  
9 therefore possible that future versions of CarbonTracker-CH<sub>4</sub> will not include  
10 estimation of ocean emissions. Note that the ocean source does not include ebullition  
11 from methane seeps and subsea permafrost (e.g. Shakhova et al., 2010). The size  
12 and variability of emissions from this source are not currently well understood, but  
13 since significant flux to the atmosphere can only occur in relatively shallow waters,  
14 this source would likely be aliased with terrestrial sources by CarbonTracker-CH<sub>4</sub>.

15

## 16 **5. Conclusions**

17

18 We have created an assimilation system for atmospheric methane,  
19 CarbonTracker-CH<sub>4</sub> and used it to estimate CH<sub>4</sub> emissions during 2000-2010 over  
20 large spatial scales. We find that simulated CH<sub>4</sub> mole fractions calculated using  
21 optimized emissions at each measurement site agree well with observations with an  
22 average bias of -10.4 ppb. Also, comparison of posterior methane profiles with  
23 measurements of CH<sub>4</sub> vertical profiles from aircraft that were not used in the  
24 assimilation show very good agreement, giving further confidence in the estimated  
25 emissions over large scales, as well as the representation of the transport processes  
26 that maintain the free-tropospheric CH<sub>4</sub> abundances. Large underestimates of CH<sub>4</sub>  
27 abundance can sometimes occur at the lower levels of the aircraft profiles in regions  
28 where there are likely strong local/regional sources that cannot be resolved by the  
29 spatial resolution of the system, are underestimated by the prior emission estimates,  
30 and/or not “seen” by other sites. This implies that use of aircraft data could supply  
31 important constraints for future inversions.

1 We have also demonstrated the diagnostic value of globally and zonally  
2 integrated CH<sub>4</sub> abundances. Comparison of observed and estimated global CH<sub>4</sub>  
3 abundances allows determination of the relative importance of prior estimates and  
4 observational constraints to the solution. Likewise, comparison of observed and  
5 posterior CH<sub>4</sub> mole fractions integrated over latitude zones indicates whether  
6 observational constraints are sufficient to capture observed temporal variability.  
7 Since the growth rate of globally and zonally integrated CH<sub>4</sub> abundance directly  
8 reflects changes in emissions and sinks, comparison of observed and simulated  
9 integrated growth provides insight into whether the inter-annual variability of fluxes is  
10 accurately recovered. Indeed we have shown that CarbonTracker-CH<sub>4</sub> is able to  
11 simulate the observed zonal average mole fractions and capture inter-annual  
12 variability in emissions quite well at high northern latitudes. In contrast,  
13 CarbonTracker-CH<sub>4</sub> is less successful in the tropics where it misses significant  
14 variability and is more influenced by prior flux estimates. This is expected given the  
15 limited number of tropical network sites and the short smoother EnKF time window.

16 CarbonTracker-CH<sub>4</sub> posterior estimates of total fluxes at high northern  
17 latitudes are about  $81 \pm 7$  Tg CH<sub>4</sub> yr<sup>-1</sup>, about 12 Tg CH<sub>4</sub> yr<sup>-1</sup> (13%) lower than prior  
18 estimates, a result that is consistent with other atmospheric inversions. Emissions  
19 from European wetlands are decreased by 30%, as found by Bergamaschi et al.  
20 (2005); however, unlike their results, emissions from wetlands in Boreal Eurasia are  
21 increased. Although CarbonTracker-CH<sub>4</sub> does not estimate increases in emissions  
22 from high northern latitudes over the decade covered by the inversion, significant  
23 inter-annual variability is recovered. During the exceptionally warm and wet summer  
24 of 2007, estimated emissions were higher than the decadal average by  $4.4 \pm 3.8$  Tg  
25 CH<sub>4</sub>. It is encouraging that CarbonTracker-CH<sub>4</sub> estimates for the Arctic agree  
26 reasonably well and within estimated uncertainties with the analysis of flux  
27 observations by McGuire et al. (2012), although they are somewhat lower ( $16 \pm 5$  Tg  
28 CH<sub>4</sub> yr<sup>-1</sup> compared to 25 Tg CH<sub>4</sub> yr<sup>-1</sup>).

29 CarbonTracker-CH<sub>4</sub> estimates for temperate latitudes are slightly increased  
30 over prior estimates, but about 10 Tg CH<sub>4</sub> yr<sup>-1</sup> is redistributed from Asia to North  
31 America, an amount that exceeds the posterior uncertainty estimate for North  
32 America ( $\pm 3.5$  Tg CH<sub>4</sub> yr<sup>-1</sup>). We used time invariant prior flux estimates for 2000

1 through 2005 when the growth rate of global atmospheric CH<sub>4</sub> was relatively small,  
2 so the assimilation does not estimate changes in natural or anthropogenic emissions.  
3 After 2006, when atmospheric CH<sub>4</sub> began to increase again, CarbonTracker-CH<sub>4</sub>  
4 allocates some of the emission increases to anthropogenic emissions at temperate  
5 latitudes, and some to tropical wetland emissions. The impact of increases in  
6 anthropogenic emissions from Asia implied by bottom up production statistics are not  
7 seen in the posterior flux estimates, but for temperate North America, the prior flux  
8 estimates are increased by about 4 Tg CH<sub>4</sub> yr<sup>-1</sup> during winter when signals from  
9 much larger biogenic emissions are small, and amount that is larger than the  
10 estimated uncertainty of 3 Tg CH<sub>4</sub> yr<sup>-1</sup>. Examination of the residuals at North  
11 American observation sites suggests that increased CH<sub>4</sub> emissions from gas and oil  
12 exploration may play a role.

13 The tropics are not currently well resolved by CarbonTracker-CH<sub>4</sub> due to  
14 sparse observational coverage and a short smoother window. However, posterior  
15 uncertainties are slightly reduced from prior uncertainties and posterior emissions are  
16 about 18% higher than prior estimates. Most of this increase is allocated to tropical  
17 South America rather than being distributed over all tropical regions. Our estimates  
18 for tropical South America are about 32 ± 4 Tg CH<sub>4</sub> yr<sup>-1</sup>, in good agreement with the  
19 analysis of Melack et al. (2004), who obtained 29 Tg CH<sub>4</sub> yr<sup>-1</sup> for the Amazon Basin.

20 As we have shown using CarbonTracker-CH<sub>4</sub>, even with the current sparse  
21 observational network it is possible to be able to draw conclusions about continental  
22 budgets of atmospheric CH<sub>4</sub> and to track and attribute variability in relatively well-  
23 sampled regions. However, information about fluxes at policy relevant scales remains  
24 elusive without increased observational coverage. This is especially true in the  
25 tropics, where droughts and flooding may have significant impact on emissions.

26

## 27 **Acknowledgements**

28 This work, including the measurements that formed the basis for the study, were funded in  
29 part by NOAA's Atmospheric Chemistry, Carbon Cycle and Climate Program. The authors  
30 would like to thank Martin Krol, Wouter Peters, Sander Houweling, Peter Bergamaschi and  
31 members of the TM5 Modeling Group for their support and helpful suggestions. The authors

1 would also like to thank Elton Chan for his helpful comments, and two anonymous reviewers  
2 for their suggestions.  
3

## 1 References

- 2 Bartlett, K. B. and R.C. Harriss, (1993), Review and assessment of methane emissions from  
3 wetlands, *Chemosphere*, 26, 1-4, 261-320, [http://dx.doi.org/10.1016/0045-](http://dx.doi.org/10.1016/0045-6535(93)90427-7)  
4 [6535\(93\)90427-7](http://dx.doi.org/10.1016/0045-6535(93)90427-7).
- 5 Beck, V., H. Chen, C. Gerbig, P. Bergamaschi, L. Bruhwiler, S. Houweling, T. Roeckmann,  
6 O. Kolle, J. Steinbach, T. Koch, C.J. Sapart, C. van der Veen, C. Frankenberg, M. O.  
7 Andreae, P. Artaxo, K.M. Longo, S.C. Wofsy, (2012), Methane airborne  
8 measurements and comparison to global models during BARCA, *J. Geophys. Res.*  
9 *117*, D15310, doi:10.1029/2011JD017345.
- 10 Bekryaev, R., I.V. Polyakov, and V. A. Alexeev, (2010) Role of polar amplification in long-  
11 term surface air temperature variations and modern Arctic warming, *J. Climate*, 23, pp.  
12 3888-3906, doi:10.1175/2010JCL13297.1.
- 13 Bergamaschi, P., S. Houweling, A. Segers, M. Krol, C. Frankenburg, R. A. Scheepmaker, E.  
14 Dlugokencky, S. C. Wofsy, E. A. Kort, C. Sweeney, T. Schuck, C. Brenninkmeijer, H.  
15 Chen, V. Beck, C. Gerbig, (2013), Atmospheric CH<sub>4</sub> in the first decade of the 21<sup>st</sup> century:  
16 Inverse modeling analysis using SCIAMACHY satellite retrievals and NOAA surface  
17 measurements, *J. Geophys. Res.*, 118, 7350-7369, doi:10.1002/jgrd.50480.
- 18 Bergamaschi, P., C. Frankenburg, J. F. Meirink, M. Krol, M. G. Villani, S. Houweling, F.  
19 Dentener, E. J. Dlugokencky, J. B., L. V. Gatti, A. Engel, I. Levin, (2009), Inverse  
20 modeling of global and regional CH<sub>4</sub> emissions using SCIAMACHY satellite retrievals, *J.*  
21 *Geophys. Res.*, 114, D22, DOI: 10.1029/2009JD012287.
- 22 Bergamaschi, P., C. Frankenburg, J.F. Meirink, M. Krol, F. Dentener, T. Wagner, U. Platt, J.  
23 O. Kaplan, S. Korner, M. Heimann, E.J. Dlugokencky, and A. Goede (2007) Satellite  
24 cartography of atmospheric methane from SCIAMACHY on board ENVISAT: 2.  
25 Evaluation based on inverse model simulations, *J. Geophys. Res.*, vol. 112,  
26 doi:10.1029/2006JD007268.
- 27 Bergamaschi, P., M. Krol, F. Dentener, A. Vermeulen, F. Meinhardt, R. Graul, M. Ramonet,  
28 W. Peters and E.J. Dlugokencky, (2005) Inverse modeling of national and European  
29 CH<sub>4</sub> emissions using the atmospheric zoom model TM5, *Atmos. Chem. Phys.*, 5,  
30 2431-2460, [www.atmos-chem-phys.org/acp/5/2431](http://www.atmos-chem-phys.org/acp/5/2431).
- 31 Bloom, A.A., P. Palmer, A. Fraser, D. Reay, and Christian Frankenberg, (2010) Large-scale  
32 controls of methanogenesis inferred from methane and gravity spaceborne data,  
33 *Science*, 327, 322-325. doi: 10.1126/science.1175176.
- 34 Bousquet, P., B. Ringeval, I.Pison, E.J. Dlugokencky, E. -G. Brunke, C. Carouge, F.  
35 Chevallier, A. Fortems-Cheiney, C. Frankenberg, D.A. Hauglustaine, P.B. Krummel,

1 R.L. Langenfelds, M. Ramonet, M. Schmidt, L.P. Steele, S. Szopa, C. Yver, N. Viovy,  
2 and P. Ciais, (2011) Source attribution of the changes in atmospheric methane for  
3 2006-2008, *Atmos. Chem. Phys.*, 11, 3689-3700, [www.atmos-chem-](http://www.atmos-chem-phys.net/11/3689/2011)  
4 [phys.net/11/3689/2011](http://www.atmos-chem-phys.net/11/3689/2011), doi:10.5194/acp-11-3689-2011.

5 Bruhwiler L.M.P., A.M. Michalak and P. Tans, Spatial and temporal resolution of carbon flux  
6 estimates for 1983–2002, *Biogeosciences*, 8, 1309-1331, doi:10.5194/bg-8-1309-  
7 2011, 2011.

8 Bruhwiler L., A.M. Michalak, W. Peters, D. Baker, and P. Tans, An improved Kalman  
9 smoother for atmospheric inversions, *Atmos. Chem Phys.*, 5, 1-12, 2005.

10 Chen, Y.-H. and Prinn, R.G., (2006) Estimation of atmospheric methane emissions between  
11 1996 and 2001 using a three-dimensional global chemical transport model, *J.*  
12 *Geophys. Res.*, 111, D10307, doi:10.1029/2005JD006058.

13 Denning, A. S., et al. (1999), Three-dimensional transport and concentration of SF<sub>6</sub> - A  
14 model intercomparison study (TransCom 2), *Tellus, Ser. B*, 51(2), 266–297.

15 Denman, K. L., Brasseur, G., Chidthaisong, A., Ciais, P., Cox, P. M., Dickinson, R. E.,  
16 Hauglustaine, D., Heinze, C., Holland, E., Jacob, D., Lohmann, U., Ramachandran,  
17 S., da Silva Dias, P. L., Wofsy, S. C., and Zhang, X.: Couplings Between Changes in  
18 the Climate System and Biogeochemistry, in: *Climate Change 2007: The Physical*  
19 *Science Basis. Contribution of Working Group I to the Fourth Assessment Report of*  
20 *the Intergovernmental Panel on Climate Change*, edited by: Solomon, S., Qin, D.,  
21 Manning, M., Chen, Z., Marquis, M., Averyt, K. B., Tignor, M., and Miller, H. L.,  
22 Cambridge University Press, Cambridge, UK and New York, NY, USA, 2007.

23 Dlugokencky, E. J., R. C. Myers, P. M. Lang, K. A. Masarie, A. M. Croswell, K. W. Thoning,  
24 B. D. Hall, J. W. Elkins and L. P. Steele, (2005), Conversion of NOAA atmospheric  
25 dry air CH<sub>4</sub> mole fractions to a gravimetrically prepared standard scale, *JGR-*  
26 *Atmospheres*, 110, D18, doi:10.1029/2005JD006035.

27 Dlugokencky, E. J., L. Bruhwiler, J. White, L. Emmons, P. Novellie, S. Montka, K. Masarie, P.  
28 Lang, A. Croswell, J. Miller, and L. Gatti (2009), Observational constraints on recent  
29 increases in the atmospheric CH<sub>4</sub> burden, *Geophys. Res. Lett.*, 36, L18803,  
30 doi:10.1029/2009GL039780.

31 Dlugokencky, E.J., Houweling, S., Bruhwiler, L., Masarie, K.A., Lang, P.M., Miller, J.B. and  
32 Tans, P.P. (2003), Atmospheric methane levels off: Temporary pause or a new  
33 steady-state? *Geophysical Research Letters* 30: 10.1029/2003GL018126.



- 1 Dlugokencky, E. J., L. P. Steele, P. M. Lang and K. A. Masarie, (1994), The growth rate and  
2 distribution of atmospheric methane, *Journal of Geophysical Research*, 99, D8, 17,  
3 doi:10.1029/94JD01245.
- 4 Etheridge, D. M., L. P. Steele, R. J. Francey, and R. L. Langenfelds (1998), Atmospheric  
5 methane between 1000 A.D. and present: Evidence of anthropogenic emissions and  
6 climatic variability, *J. Geophys. Res.*,103(D13), 15,979–15,993, doi:10.1029/  
7 98JD00923.
- 8 European Commission, Joint Research Centre (JRC)/Netherlands Environmental  
9 Assessment Agency (PBL). Emission Database for Global Atmospheric Research  
10 (EDGAR), release version 4.0. <http://edgar.jrc.ec.europa.eu>, 2009.
- 11 Forster, P., Ramaswamy, V., Artaxo, P., Bernsten, T., Betts, R., Fahey, D. W., Haywood, J.,  
12 Lean, J., Lowe, D. C., Myhre, G., Nganga, J., Prinn, R., and Raga, G., M. S. a. R. V.  
13 D.: Changes in Atmospheric Constituents and in Radiative Forcing, in: Cli- mate  
14 Change 2007: The Physical Science Basis. Contribution of Working Group I to the  
15 Fourth Assessment Report of the Inter- governmental Panel on Climate Change,  
16 edited by: Solomon, S., Qin, D., Manning, M., Chen, Z., Marquis, M., Averyt, K. B.,  
17 Tignor, M., and Miller, H. L., Cambridge University Press, Cam- bridge, UK and New  
18 York, NY, USA, 2007.
- 19 Frohling, S., et al. (2011), Peatlands in the Earth's 21<sup>st</sup> century climate system, *Environ.*  
20 *Rev.*, 19, 371-396, doi:10.1139/A11-014.
- 21 Giglio, L., G. R. van der Werf, J. T. Randerson, G. J. Collatz, and P. Kasibhatla, (2006),  
22 Global estimation of burned area using MODIS active fire observations, *Atmos.*  
23 *Chem. Phys.*, 6, 957-974, 2006, doi:10.5194/acp-6-957-2006.
- 24 Gurney, K., R. Law, P. Rayner, and S. Denning, “TransCom 3 Experimental Protocol,”  
25 Department of Atmospheric Science, Colorado State University, paper no. 707, July  
26 2000.
- 27 Hansen, J. R. Ruedy, M. Sato, and K. Lo, (2010), Global surface temperature change, *Rev.*  
28 *Geophys.*, 48, RG4004, doi:10.1029/2010RG000345.
- 29 Harden, J.W., C. Koven, C. Ping, G. Hugelius, A. D. McGuire, P. Camill, T. Jorgenson, P.  
30 Kuhry, G.J. Michaelson, J. O'Donnell, E.A. Schuur, C. Tarnocai, K. Johnson, G.  
31 Grosse, (2012), Field information links permafrost carbon to physical vulnerabilities of  
32 thawing, *Geophys. Res. Lett.*, 39, L15704, doi:10.1029/2012GL051958.
- 33 Hein, R., Crutzen, P. J., and Heimann, M.: An inverse modeling approach to investigate the

1 global atmospheric methane cycle, *Global. Biogeochem. Cy.*, 11, 43–76, 1997.

2 Hofmann, D. J., J. H. Butler, E. J. Dlugokencky, J. W. Elkins, K. Masarie, S. A. Montzka, and  
3 P. Tans, (2006a), The role of carbon dioxide in climate forcing from 1979 - 2004:  
4 Introduction of the Annual Greenhouse Gas Index, *Tellus B*, 58B, 614-619.

5 Houtekamer, P.L., and H.L. Mitchell (1998), Data assimilation using an ensemble Kalman  
6 filter technique, *Mon. Weather. Rev.*, 126(3), 796-811.

7 Houweling, S., Krol, M., Bergamaschi, P., Frankenberg, C., Dlugokencky, E. J., Morino, I.,  
8 Notholt, J., Sherlock, V., Wunch, D., Beck, V., Gerbig, C., Chen, H., Kort, E. A.,  
9 Röckmann, T., and Aben, I.: A multi-year methane inversion using SCIAMACHY,  
10 accounting for systematic errors using TCCON measurements, *Atmos. Chem. Phys.*,  
11 14, 3991-4012, doi:10.5194/acp-14-3991-2014, 2014.

12 Houweling, S., T. Kaminski, F. Dentener, J. Lelieveld, M. Heimann, (1999), Inverse modeling  
13 of methane sources and sinks using the adjoint of a global transport model, *J.*  
14 *Geophys. Res.*, 104, D21, DOI: 10.1029/1999JD900428.

15 Kaminski, T., P.J. Rayner, M. Heimann, and I.G. Enting, (2001), On aggregation errors in  
16 atmospheric transport inversions, *J. Geophys. Res.* 106(D5), 4703-4715.

17 Kaplan, J. O., (2002), Wetlands at the last glacial maximum: Distribution and methane  
18 emissions, *Geophys. Res. Lett.*, 29(6), 1079, doi:10.1029/2001GL013366.

19 Karion, Anna, Colm Sweeney, Gabrielle Pétron, Gregory Frost, R. Michael Hardesty,  
20 Jonathan Kofler, Ben R. Miller, Tim Newberger, Sonja Wolter, Robert Banta, Alan  
21 Brewer, Ed Dlugokencky, Patricia Lang, Stephen A. Montzka, Russell Schnell, Pieter  
22 Tans, Michael Trainer, Robert Zamora and Stephen Conley, (2013), Methane  
23 emissions estimate from airborne measurements over a western United States  
24 natural gas field, *Geophysical Research Letters*, 10.1002/grl.50811.

25 Krol, M., S. Houweling, B. Bregman, M. van den Broek, A. Segers, P. van Velthoven,  
26 W. Peters, F. Dentener, and P. Bergamaschi, (2005), The two-way nested global  
27 chemistry-transport zoom model TM5: algorithm and applications, *Atmos. Chem.*  
28 *Phys.*, 5, 417-432, doi:10.5194/acp-5-417-2005.

29 Krol, M., J. Lelieveld, (2003), Can the variability in tropospheric OH be deduced from  
30 measurements of 1,1,1-trichloroethane (methyl chloroform)?, *J. Geophys. Res.*, 108,  
31 D3, DOI: 10.1029/2002JD002423.

32 Louergue, L., A. Schilt, R. Spahni, V. Masson-Delmotte, T. Blunier, B. Lemieux, J.-M.  
33 Barnola, D. Raynaud, T. F. Stocker and J. Chappellaz, (2008) Orbital and millennial-

1 scale features of atmospheric CH<sub>4</sub> over the past 800,000 years, *Nature*, 453, 383-  
2 386, doi10.1038/nature06950.

3 Masarie, K. A. and P. P. Tans, (1995), Extension and integration of atmospheric carbon  
4 dioxide data into a globally consistent measurement record, *Journal of Geophysical*  
5 *Research-Atmospheres*, 100, D6, 11593-11610.

6 Matthews, E., Fung, I., and Lerner, J.: Methane emission from rice cultivation: Geographic  
7 and seasonal distribution of cultivated areas and emissions, *Global Biogeochem.*  
8 *Cycles*, 5, 3–24, 1991.

9 Matthews, E., 1989: *Global Data Bases on Distribution, Characteristics and Methane*  
10 *Emission of Natural Wetlands: Documentation of Archived Data Tape*. NASA TM-  
11 4153. National Aeronautics and Space Administration.

12 McGuire, A.D., T.R. Christensen, D. Hayes, A. Heroult, E. Euskirchen, J.S. Kimball, C.  
13 Koven, P. Laflour, P.A. Miller, W. Oechel, P. Peylin, M. Williams, and Y. Yi, (2012) An  
14 assessment of the carbon balance of Arctic tundra: comparisons among  
15 observations, process models, and atmospheric inversions, *Biogeosci.*, 9, 3185-3204,  
16 doi:10.5194/bg-9-3185-2012.

17 Melack, J.M., L. L. Hess, M. Gastil, B. R. Forsberg, S. K. Hamilton, I. B.T. Lima and E.  
18 M.L.M. Novo, (2004), Regionalization of methane emissions in the Amazon Basin  
19 with microwave remote sensing, *Global Change Biology* 10, 530–544, doi:  
20 10.1111/j.1529-8817.2003.00763.x.

21 Melton, J.R., R. Wania, E.L. Hodson, B. Poulter, B. Ringeval, R. Spahni, T. Bohn, C.A. Avis,  
22 D.J. Beerling, G. Chen, A.V. Eliseev, S.N. Denisov, P.O. Hopcroft, D.P. Lettenmaier,  
23 W.J. Riley, J.S. Singarayer, Z.M Subin, H.Tian, S. Zurcher, V. Brovkin, P.M. van  
24 Bodegom, T. Kleinen, Z.C. Yu, and J.O. Kaplan (2013), Present state of global  
25 wetland extent and wetland methane modelling: conclusions from a model  
26 intercomparison project (WETCHIMP), *Biogeosciences* 10, 753-788, doi:10.5194/bg-  
27 10-753-2013.

28 Miller, J. B., K.A. Mack, R. Dissly, J.W.C. White, E. J. Dlugokencky and P. P. Tans, (2002),  
29 Development of analytical methods and measurements of <sup>13</sup>C/<sup>12</sup>C in atmospheric  
30 CH<sub>4</sub> from the NOAA Climate Monitoring and Diagnostics Laboratory Global Air  
31 Sampling Network, *Journal of Geophysical Research-Atmospheres*, 107, d13, 4178,  
32 doi:10.1029/2001JD000630.

- 1 Miller, J. B., Gatti, L. V., D'Amelio, M. T. S., Crotwell, A., Dlugokencky, E., Bakwin, P. S.,  
2 Artaxo, P., and Tans, P.: Airborne sampling reveals large methane enhancement over  
3 the Amazon basin, *Geophys. Res. Lett.*, 34, 2007.
- 4 Miller, Scot M., Steven C. Wofsy, Anna M. Michalak, Eric A. Kort, Arlyn E. Andrews,  
5 Sebastien C. Biraud, Edward J. Dlugokencky, Janusz Eluszkiewicz, Marc L. Fischer,  
6 Greet Janssens-Maenhout, Ben R. Miller, John B. Miller, Stephen A. Montzka,  
7 Thomas Nehrkorn, and Colm Sweeney (2013), Anthropogenic emissions of methane  
8 in the United States, *PNAS* 110 (50) 20018-20022, doi:10.1073/pnas.1314392110.
- 9 Mikaloff Fletcher, S. E., P. P. Tans, L. M. Bruhwiler, J. B. Miller, and M. Heimann (2004a),  
10 CH<sub>4</sub> sources estimated from atmospheric observations of CH<sub>4</sub> and its <sup>13</sup>C/<sup>12</sup>C isotopic  
11 ratios: 1. Inverse modeling of source processes, *Global Biogeochem. Cycles*, 18,  
12 GB4004, doi:10.1029/2004GB002223.
- 13 Mikaloff Fletcher, S. E., P. P. Tans, L. M. Bruhwiler, J. B. Miller, and M. Heimann (2004b),  
14 CH<sub>4</sub> sources estimated from atmospheric observations of CH<sub>4</sub> and its <sup>13</sup>C/<sup>12</sup>C isotopic  
15 ratios: 2. Inverse modeling of CH<sub>4</sub> fluxes from geographical regions, *Global*  
16 *Biogeochem. Cycles*, 18, GB4005, doi:10.1029/2004GB002224.
- 17 Montzka, S.A., M. Krol, E. Dlugokencky, B. Hall, P. Jockel, J. Lelieveld, (2011), Small  
18 Interannual Variability of Global Atmospheric Hydroxyl, *Science*, 331, 6013, pp. 67-  
19 69, DOI: 10.1126/science.1197640.
- 20 Myhre, G., D. Shindell, F.-M. Bréon, W. Collins, J. Fuglestedt, J. Huang, D. Koch, J.-F.  
21 Lamarque, D. Lee, B. Mendoza, T. Nakajima, A. Robock, G. Stephens, T. Takemura  
22 and H. Zhang, 2013: Anthropogenic and Natural Radiative Forcing. In: *Climate*  
23 *Change 2013: The Physical Science Basis. Contribution of Working Group I to the*  
24 *Fifth Assessment Report of the Intergovernmental Panel on Climate Change* [Stocker,  
25 T.F., D. Qin, G.-K. Plattner, M. Tignor, S.K. Allen, J. Boschung, A. Nauels, Y. Xia,  
26 V. Bex and P.M. Midgley (eds.)]. Cambridge University Press, Cambridge, United  
27 Kingdom and New York, NY, USA.
- 28 Peters, W., A.R. Jacobson, C. Sweeney, A. Andrews, T. J. Conway, K. A. Masarie, J. B.  
29 Miller, L. Bruhwiler, G. Petron, A. Hirsch, D. Worthy, G. van der Werf, J. T.  
30 Randerson, P. Wennberg, M. Krol and P. P. Tans, (2007), An atmospheric perspective  
31 on North American carbon dioxide exchange: CarbonTracker, *Proceedings of the*  
32 *National Academy of Sciences*, 104, 48, 18925-18930, 10.1073/pnas.0708986104.

- 1 Peters, W., J. B. Miller, J. Whitaker, A. S. Denning, A. Hirsch, M. C. Krol, D. Zupanski, L.  
2 Bruhwiler, P. P. Tans, (2005), An ensemble data assimilation system to estimate CO<sub>2</sub>  
3 surface fluxes from atmospheric trace gas observations, *J. Geophys. Res.*, *110*, D24,  
4 DOI: 10.1029/2005 JD006157.
- 5 Peters, W, M. C. Krol, E. J. Dlugokencky, F. J. Dentener, P. Bergamaschi, G. Dutton, P. v.  
6 Velthoven, J. B. Miller, L. Bruhwiler, P. P. Tans, (2004), Toward regional-scale  
7 modeling using the two-way nested global model TM5: Characterization of transport  
8 using SF<sub>6</sub>, *J. Geophys. Res.*, *109*, D19, DOI: 10.1029/2004JD005020.
- 9 Pétron, Gabrielle, G. Frost, B. R. Miller, A. I. Hirsch, S. A. Montzka, A. Karion, M. Trainer, C.  
10 Sweeney, A. E. Andrews, L. Miller, J. Kofler, A. Bar-Ilan, E. J. Dlugokencky, L.  
11 Patrick, C. T. Moore Jr., T. B. Ryerson, C. Siso, W. Kolodzey, P. M. Lang, T. Conway,  
12 P. Novelli, K. Masarie, B. Hall, D. Guenther, D. Kitzis, J. Miller, D. Welsh, D. Wolfe,  
13 W. Neff, P. Tans, (2012), Hydrocarbon emissions characterization in the Colorado  
14 Front Range: A pilot study, *J. Geophys. Res.*, v117, D4,  
15 DOI: 10.1029/2011JD016360.
- 16 Rayner, P. J., M. Scholze, W. Knorr, T. Kaminski, R. Giering, and H. Widmann (2005), Two  
17 decades of terrestrial carbon fluxes from a carbon cycle data assimilation system  
18 (CCDAS), *Global Biogeochem. Cycles*, *19*, GB2026, doi:10.1029/2004GB002254.
- 19 Rhee, T.S., A.J. Kettle, and M.O. Andreae, (2009), Methane and nitrous oxide emissions  
20 from the ocean: A reassessment using basin-wide observations in the Atlantic, *J.*  
21 *Geophys. Res.*, *114*, D12304, doi:10.1029/2008JD011662.
- 22 Ridgwell, A. J., S. J. Marshall, K. Gregson, (1999), Consumption of atmospheric methane by  
23 soils: A process-based model, *G.B.C.*, *13*, 1, 59-70, DOI: 10.1029/1998GB900004.
- 24 Rigby, M., Prinn, R. G., Fraser, P. J., Simmonds, P. G., Lan- genfelds, R. L., Huang, J.,  
25 Cunnold, D. M., Steele, L. P., Krummel, P. B., Weiss, R. F., O'Doherty, S., Salameh,  
26 P. K., Wang, H. J., Harth, C. M., Muhle, J., and Porter, L. W.: Re-  
27 newed growth of  
28 atmospheric methane, *Geophys. Res. Lett.*, *35*, L22805, doi:10.1029/2008gl036037,
- 29 Sanderson, M.G., (1996), Biomass of termites and their emissions of methane and carbon  
30 dioxide: A global database, *G.B.C.*, *10*, 4, 543-557, DOI: 10.1029/96GB01893.
- 31 Shakhova, N., I. Semilitov, I. Leifer, V. Sergienko, A., Salyuk, D. Kosmach, D. Chernykh, C.  
32 Stubbs, D. Nicolsky, V. Tumskoy, O. Gustafsson, (2013) Ebullition and storm-induced  
33 methane release from the East Siberian Arctic Shelf, *Nat. Geosci.*, *7*, 64-70,

1 doi:10.1038/ngeo2007.

2 Schaefer, Kevin, Tingjun Zhang, Lori Bruhwiler, Andrew P. Barrett (2010) Strength and  
3 timing of the permafrost carbon feedback, *Tellus B*, 63B, 165-180, doi:10.1111/j.1600-  
4 0889.2011.00527.x, 2011.

5 Schuur, E.A., B. Abbott, and the Permafrost Carbon Network, (2011) High Risk of Permafrost  
6 Thaw, *Nature*, 32, vol. 480.

7 Spahni, R., R. Wania, L. Neef, M. van Weele, I. Pison, P. Bousquet, C. Frankenberg, P.N.  
8 Foster, F. Joos, I.C. Prentice, and P. van Velthoven, Constraining global methane  
9 emissions and uptake by ecosystems, *Biogeosciences*, 8, 1643-1665, 2011,  
10 doi:10.5194/bg-8-1643-2011.

11 Stroeve, J., M. Serreze, S. Drobot, S. Gearheard, M. Holland, J. Maslanik, W. Meier, T.  
12 Scambos, 2008. Arctic Sea Ice Extent Plummetts in 2007. *Eos, Transactions,*  
13 *American Geophysical Union* 89(2): 13-14, doi:10.1029/2008EO020001.

14 Tarnocai, C., J. G. Canadell, E. A. G. Schuur, P. Kuhry, G. Mazhitova, and S. Zimov (2009),  
15 Soil organic carbon pools in the northern circumpolar permafrost region, *Global*  
16 *Biogeochem. Cycles*, 23, GB2023, doi:10.1029/2008GB003327.

17 Walter, B. P. and Heimann, M., A process-based, climate-sensitive model to derive methane  
18 emissions from natural wetlands: Application to five wetland sites, sensitivity to  
19 model parameters, and climate, *Global Biogeochem. Cycles*, 14, 3, 745–765, 2000.

20 Walter Anthony, K., L. C. Smith and F. S. Chapin III, (2007) Methane bubbling from northern  
21 lakes: present and future contributions to the global methane budget, *Phil. Trans. R.*  
22 *Soc. A.*, 365, 1657-1676, DOI:10.1098/rsta.2007.2036.

23 Walter Anthony, K., P. Anthony, G. Grosse and J. Chanton, (2012) Geologic methane seeps  
24 along boundaries of Arctic permafrost thaw and melting glaciers, *Nature GeoSci.*, 5,  
25 419-426, DOI:10.1038/NCEO1480.

26 van der Werf, G.R., J. T. Randerson, L. Giglio, G. J. Collatz, P. S. Kasibhatla, and A. F.  
27 Arellano, Jr., (2006), Interannual variability in global biomass burning emissions from  
28 1997 to 2004, *Atmos. Chem. Phys.*, 6, 3423–3441, [www.atmos-chem-](http://www.atmos-chem-phys.net/6/3423/2006/)  
29 [phys.net/6/3423/2006/](http://www.atmos-chem-phys.net/6/3423/2006/).

30 Whitaker, J.S. and T.M. Hamill, (2002), Ensemble Data Assimilation without Perturbed  
31 Observations, *Mon. Wea. Rev.*, 130, 1913–1924, doi: [http://dx.doi.org/10.1175/1520-](http://dx.doi.org/10.1175/1520-0493(2002)130<1913:EDAWPO>2.0.CO;2)  
32 [0493\(2002\)130<1913:EDAWPO>2.0.CO;2](http://dx.doi.org/10.1175/1520-0493(2002)130<1913:EDAWPO>2.0.CO;2).

33 Yan X., H. Akiyama, K. Yagi, H. Akimoto, (2009), Global estimations of the inventory and

1 mitigation potential of methane emissions from rice cultivation conducted using the  
2 2006 Intergovernmental Panel on Climate Change Guidelines, *G.B.C.*, 23, 2,  
3 DOI: 10.1029/2008GB003299.

4 Shakhova, N., I. Semilitov, A. Salyuk, V. Yusupov, D. Kosmach, O. Gustafsson, (2010)  
5 Extensive venting the atmosphere from sediments of the East Siberian Arctic shelf,  
6 *Science*, 5, Vol. 327 no. 5970 pp. 1246-1250 DOI: 10.1126/science.1182221.

7 Schaefer, Kevin, Tingjun Zhang, Lori Bruhwiler, Andrew P. Barrett (2010) Strength and  
8 timing of the permafrost carbon feedback, *Tellus B*, 63B, 165-180,doi:10.1111/j.1600-  
9 0889.2011.00527.x, 2011.

10 Schuur, E.A., B. Abbott, and the Permafrost Carbon Network, (2011) High Risk of Permafrost  
11 Thaw, *Nature*, 32, vol. 480.

12 Spahni, R., R. Wania, L. Neef, M. van Weele, I. Pison, P. Bousquet, C. Frankenberg, P.N.  
13 Foster, F. Joos, I.C. Prentice, and P. van Velthoven, Constraining global methane  
14 emissions and uptake by ecosystems, *Biogeosciences*, 8, 1643-1665, 2011,  
15 doi:10.5194/bg-8-1643-2011.

16 Stroeve, J., M. Serreze, S. Drobot, S. Gearheard, M. Holland, J. Maslanik, W. Meier, T.  
17 Scambos, 2008. Arctic Sea Ice Extent Plummetts in 2007. *Eos, Transactions,*  
18 *American Geophysical Union* 89(2): 13-14, doi:10.1029/2008EO020001.

19 Tarnocai, C., J. G. Canadell, E. A. G. Schuur, P. Kuhry, G. Mazhitova, and S. Zimov (2009),  
20 Soil organic carbon pools in the northern circumpolar permafrost region, *Global*  
21 *Biogeochem. Cycles*, 23, GB2023, doi:10.1029/2008GB003327.

22 Walter, B. P. and Heimann, M., A process-based, climate-sensitive model to derive methane  
23 emissions from natural wetlands: Application to five wetland sites, sensitivity to  
24 model parameters, and climate, *Global Biogeochem. Cycles*, 14, 3, 745–765, 2000.

25 Walter Anthony, K., L. C. Smith and F. S. Chapin III, (2007) Methane bubbling from northern  
26 lakes: present and future contributions to the global methane budget, *Phil. Trans. R.*  
27 *Soc. A.*, 365, 1657-1676, DOI:10.1098/rsta.2007.2036.

28 Walter Anthony, K., P. Anthony, G. Grosse and J. Chanton, (2012) Geologic methane seeps  
29 along boundaries of Arctic permafrost thaw and melting glaciers, *Nature GeoSci.*, 5,  
30 419-426, DOI:10.1038/NGEO1480.

31 van der Werf, G.R., J. T. Randerson, L. Giglio, G. J. Collatz, P. S. Kasibhatla, and A. F.  
32 Arellano, Jr., (2006), Interannual variability in global biomass burning emissions from  
33 1997 to 2004, *Atmos. Chem. Phys.*, 6, 3423–3441, [www.atmos-chem-](http://www.atmos-chem-phys.net/6/3423/2006/)

1 [phys.net/6/3423/2006/](http://phys.net/6/3423/2006/).

2 Whitaker, J.S. and T.M. Hamill, (2002), Ensemble Data Assimilation without Perturbed  
3 Observations, *Mon. Wea. Rev.*, **130**, 1913–1924, doi: [http://dx.doi.org/10.1175/1520-0493\(2002\)130<1913:EDAWPO>2.0.CO;2](http://dx.doi.org/10.1175/1520-0493(2002)130<1913:EDAWPO>2.0.CO;2).

5 Yan X., H. Akiyama, K. Yagi, H. Akimoto, (2009), Global estimations of the inventory and  
6 mitigation potential of methane emissions from rice cultivation conducted using the  
7 2006 Intergovernmental Panel on Climate Change Guidelines, *G.B.C.*, **23**, 2,  
8 DOI: 10.1029/2008GB003299.

9

10

11

12

13

14

15

16

17

18

19

20

21

22

23

24

25



1  
2  
3  
4  
5  
6  
7  
8  
9  
10  
11  
12  
13  
14  
15  
16  
17  
18  
19  
20

Table 1 – CarbonTracker-CH<sub>4</sub> data preprocessing.

Measurement Program	Data Preprocessing
ESRL discrete surface	All valid* data. Multiple values from the same day and location are averaged. No sample time-of-day restriction (see exception below).
EC in situ sites	All valid data from highest intake. Day average using 12-16 LST.

\* In this context "Valid Data" means the observation is thought to be free of sampling and analytical problems and has not been locally influenced.

1  
2  
3  
4  
5  
6  
7  
8  
9  
10  
11  
12  
13  
14  
15

Table 2- Summary of the observation sites used in CarbonTracker-CH<sub>4</sub>, and the performance of the assimilation scheme at each site. “#Obs.” and “#Rej.” are the number of observations available and the number of observations for which the prior simulated concentrations deviate more than 3σ from the observations using a normal distribution defined with the observed value as the mean and the model-data mismatch error (MDM) as the standard deviation. The bias is the long-term mean of the posterior residuals (simulated-observed), σ is the standard deviation of the residuals for each site, and C<sub>2</sub> is the chi-squared statistic calculated as the mean residual divided by the prior uncertainty (Simulated-Observed/(HQH+R); where H is the matrix of transport response, Q is the prior flux uncertainty and R is the model-data mismatch error).

Site Code	Lab	Lat.	Lon.	Elev. masl	# Obs.	# Rej.	MDM ppb	Bias ppb	σ ppb	χ <sup>2</sup>
abp_01d0	ESRL	12.77S	38.17W	1.0	112	3	7.5	-8.4	7.7	2.0
alt_01d0	ESRL	82.45N	62.51W	200.0	532	0	15.0	-2.2	8.7	0.3
alt_06c0	EC	82.45N	62.51W	200.0	3181	10	15.0	-1.2	10.2	0.4
amt_01d0	ESRL	45.03N	68.68W	50.0	267	4	30.0	-6.1	22.8	0.4
amt_01p0	ESRL	45.03N	68.68W	50.0	174	0	30.0	0.8	16.5	0.3
asc_01d0	ESRL	7.97S	14.4W	74.5	961	79	7.5	-10.0	9.3	3.0
ask_01d0	ESRL	23.18N	5.42E	2728.0	491	0	25.0	-6.9	9.1	0.2
azr_01d0	ESRL	38.77N	27.38W	40.0	350	16	15.0	-12.0	15.9	1.7
bal_01d0	ESRL	55.35N	17.22E	3.0	974	0	75.0	1.4	29.4	0.1
bhd_01d0	ESRL	41.41S	174.87E	85.0	165	0	7.5	-4.1	5.4	0.7

bkt_01d0	ESRL	0.2S	100.32E	864.5	345	0	75.0	6.8	30.8	0.2
bme_01d0	ESRL	32.37N	64.65W	30.0	256	14	15.0	-13.6	17.4	2.1
bmw_01d0	ESRL	32.27N	64.88W	30.0	352	7	15.0	-13.2	12.8	1.4
brw_01d0	ESRL	71.32N	156.61W	11.0	514	13	15.0	-5.8	16.1	1.1
bsc_01d0	ESRL	44.17N	28.68E	3.0	501	1	75.0	-14.4	56.2	0.5
cba_01d0	ESRL	55.21N	162.72W	21.34	892	23	15.0	-10.6	13.4	1.1
cdl_06c0	EC	53.99N	105.12W	600.0	1390	77	25.0	-24.7	30.3	2.1
ego_01d0	ESRL	40.68S	144.69E	94.0	416	0	7.5	-4.1	4.6	0.6
chr_01d0	ESRL	1.7N	157.17W	3.0	426	79	7.5	-14.6	9.9	5.2
crz_01d0	ESRL	46.45S	51.85E	120.0	453	0	7.5	-2.9	4.3	0.5
egb_06c0	EC	44.23N	79.78W	251.0	1810	0	75.0	-6.9	28.7	0.1
eic_01d0	ESRL	27.15S	109.45W	50.0	323	3	7.5	-7.3	5.3	1.4
esp_06c0	EC	49.58N	126.37W	7.0	403	0	25.0	-6.8	12.3	0.3
etl_06c0	EC	54.35N	104.98W	492.0	1780	135	25.0	-30.1	31.9	2.8
fsd_06c0	EC	49.88N	81.57W	210.0	3409	10	25.0	-9.4	18.3	0.6
gmi_01d0	ESRL	13.43N	144.78E	3.0	802	11	15.0	-10.2	13.0	1.2
hba_01d0	ESRL	75.58S	26.5W	30.0	506	0	7.5	0.5	4.6	0.3
hpb_01d0	ESRL	47.8N	11.01E	985.0	241	17	25.0	-13.8	35.7	1.4
hun_01d0	ESRL	46.95N	16.65E	248.0	530	3	75.0	-14.0	43.7	0.3
ice_01d0	ESRL	63.4N	20.29W	118.0	529	7	15.0	-3.3	13.1	0.6
izo_01d0	ESRL	28.31N	16.5W	2360.0	443	2	15.0	-8.5	11.4	0.9
key_01d0	ESRL	25.67N	80.16W	3.0	388	3	25.0	-7.0	20.1	0.6
kum_01d0	ESRL	19.52N	154.82W	3.0	720	42	7.5	-6.8	10.6	2.2
kzd_01d0	ESRL	44.06N	76.82E	601.0	454	4	75.0	5.2	44.0	0.2

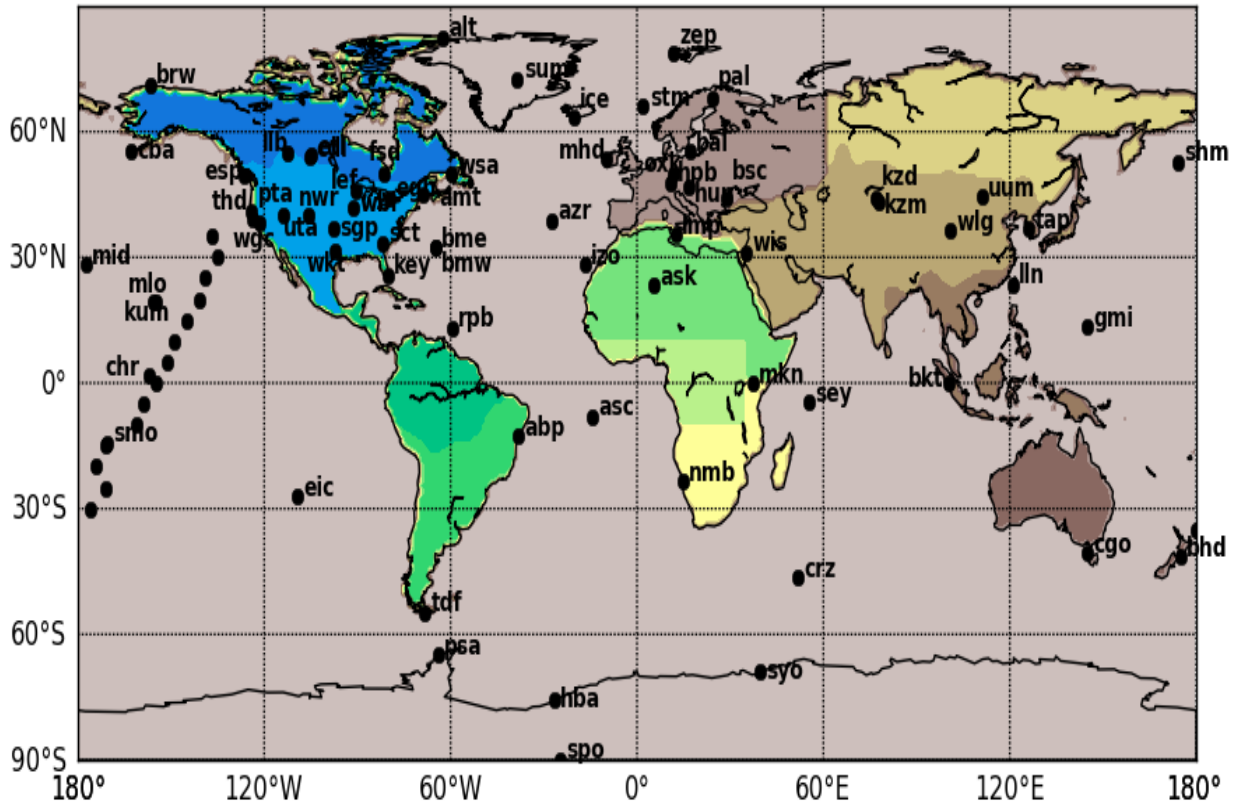
kzm_01d0	ESRL	43.25N	77.88E	2519.0	447	2	25.0	-2.8	20.2	0.6
lef_01d0	ESRL	45.95N	90.27W	472.0	505	6	30.0	-9.7	28.6	0.8
lef_01p0	ESRL	45.95N	90.27W	472.0	341	7	30.0	-2.1	30.9	0.9
llb_06c0	EC	54.95N	112.45W	540.0	1152	84	75.0	-79.9	122.4	3.7
lln_01d0	ESRL	23.47N	120.87E	2862.0	222	1	25.0	-4.1	24.4	0.9
lmp_01d0	ESRL	35.52N	12.62E	45.0	206	1	25.0	-0.7	20.5	0.5
mhd_01d0	ESRL	53.33N	9.9W	5.0	416	0	25.0	-4.6	11.4	0.2
mid_01d0	ESRL	28.21N	177.38W	3.7	525	5	15.0	-10.7	10.9	1.0
mkn_01d0	ESRL	0.05S	37.3E	3897.0	146	0	25.0	-14.3	14.8	0.7
mlo_01d0	ESRL	19.54N	155.58W	3397.0	565	0	15.0	-2.4	10.9	0.5
nmb_01d0	ESRL	23.58S	15.03E	456.0	164	0	25.0	-7.8	11.4	0.3
nwr_01d0	ESRL	40.05N	105.58W	3523.0	543	18	15.0	-11.1	15.2	1.5
oxk_01d0	ESRL	50.03N	11.8E	1022.0	202	2	75.0	-12.5	42.9	0.3
pal_01d0	ESRL	67.97N	24.12E	560.0	377	54	15.0	16.7	35.1	0.2
poc000_01d1	ESRL	0.0N	155.0W	10.0	173	33	7.5	-13.9	9.5	4.7
pocn05_01D1	ESRL	5.0N	151.0W	10.0	174	29	7.5	-15.1	9.5	5.3
pocn10_01D1	ESRL	10.0N	149.0W	10.0	174	45	7.5	-16.0	14.0	7.6
pocn15_01D1	ESRL	15.0N	145.0W	10.0	168	26	7.5	-11.0	11.1	4.1
pocn20_01D1	ESRL	20.0N	141.0W	10.0	166	13	7.5	-6.8	11.5	2.9
pocn25_01D1	ESRL	25.0N	139.0W	10.0	155	14	7.5	-7.0	11.2	2.6
pocn30_01D1	ESRL	30.0N	135.0W	10.0	153	18	7.5	-4.7	13.9	2.7
pocn35_01D1	ESRL	35.0N	137.0W	10.0	5	0	7.5	-4.0	8.6	1.4
pocs05_01D1	ESRL	5.0S	159.0W	10.0	159	31	7.5	-15.3	8.6	5.2
pocs10_01D1	ESRL	10.0S	161.0W	10.0	170	41	7.5	-14.6	10.1	5.4

pocs15_01D1	ESRL	15.0S	171.0W	10.0	163	15	7.5	-10.4	9.5	3.4
pocs20_01D1	ESRL	20.0S	174.0W	10.0	169	8	7.5	-7.3	7.9	2.0
pocs25_01D1	ESRL	25.0S	171.0W	10.0	164	0	7.5	-5.3	6.3	1.1
pocs30_01D1	ESRL	30.0S	176.0W	10.0	166	0	7.5	-5.0	5.0	0.8
pocs35_01D1	ESRL	35.0S	180.0E	10.0	14	1	7.5	-0.5	8.2	0.5
psa_01d0	ESRL	64.92S	64.0W	10.0	542	0	7.5	-2.7	3.7	0.3
pta_01d0	ESRL	38.95N	123.74W	17.0	427	1	25.0	-4.6	16.9	0.4
rpb_01d0	ESRL	13.17N	59.43W	45.0	519	2	15.0	-10.7	10.0	0.9
sct_01p0	ESRL	33.41N	81.83W	115.2	351	0	75.0	-23.5	33.7	0.3
sey_01d0	ESRL	4.67S	55.17E	3.0	514	43	7.5	-6.5	12.3	3.1
sgp_01d0	ESRL	36.8N	97.5W	314.0	443	10	75.0	-56.1	57.4	0.8
shm_01d0	ESRL	52.72N	174.1E	40.0	482	0	25.0	-8.7	11.4	0.3
smo_01d0	ESRL	14.25S	170.56W	42.0	568	70	7.5	-10.5	9.9	3.6
spo_01d0	ESRL	89.98S	24.8W	2810.0	566	0	7.5	-4.1	4.7	0.7
stm_01d0	ESRL	66.0N	2.0E	0.0	917	9	15.0	-1.4	13.5	0.5
sum_01d0	ESRL	72.58N	38.48W	3238.0	468	0	15.0	-4.7	8.4	0.4
syo_01d0	ESRL	69.0S	39.58E	11.0	260	0	7.5	-2.6	3.6	0.3
tap_01d0	ESRL	36.73N	126.13E	20.0	441	3	75.0	10.2	61.7	0.5
tdf_01d0	ESRL	54.87S	68.48W	20.0	206	0	7.5	-4.2	4.1	0.6
thd_01d0	ESRL	41.05N	124.15W	107.0	400	0	25.0	-7.0	14.6	0.4
uta_01d0	ESRL	39.9N	113.72W	1320.0	525	12	25.0	-5.5	28.7	0.4
uum_01d0	ESRL	44.45N	111.1E	914.0	533	1	25.0	-1.2	22.7	0.3
wbi_01p0	ESRL	41.72N	91.35W	241.7	296	12	30.0	-8.3	38.0	1.4
wgc_01p0	ESRL	38.27N	121.49W	0.0	339	53	75.0	-118.	158.8	6.9

wis_01d0	ESRL	31.13N	34.88E	400.0	552	3	25.0	-6.2	23.7	0.8
wkt_01d0	ESRL	31.31N	97.33W	251.0	409	55	30.0	-48.6	43.7	3.8
wkt_01p0	ESRL	31.31N	97.33W	251.0	298	38	30.0	-46.7	58.7	5.8
wlg_01d0	ESRL	36.29N	100.9E	3810.0	462	17	15.0	-1.8	20.6	0.8
wsa_06c0	EC	49.93N	60.02W	5.0	2314	52	25.0	3.8	25.5	0.9
zep_01d0	ESRL	78.9N	11.88E	475.0	588	11	15.0	2.2	14.2	0.5

- 1
- 2
- 3
- 4
- 5
- 6
- 7
- 8
- 9
- 10
- 11
- 12
- 13
- 14
- 15
- 16
- 17
- 18
- 19

1



2

3

4

5 **Figure 1** - Map showing locations of observations used in CarbonTracker-CH<sub>4</sub>.  
6 Shading indicates the boundaries of the Transcom 3 source regions (Gurney et al.,  
7 2000) with an additional tropical African region.

8

9

10

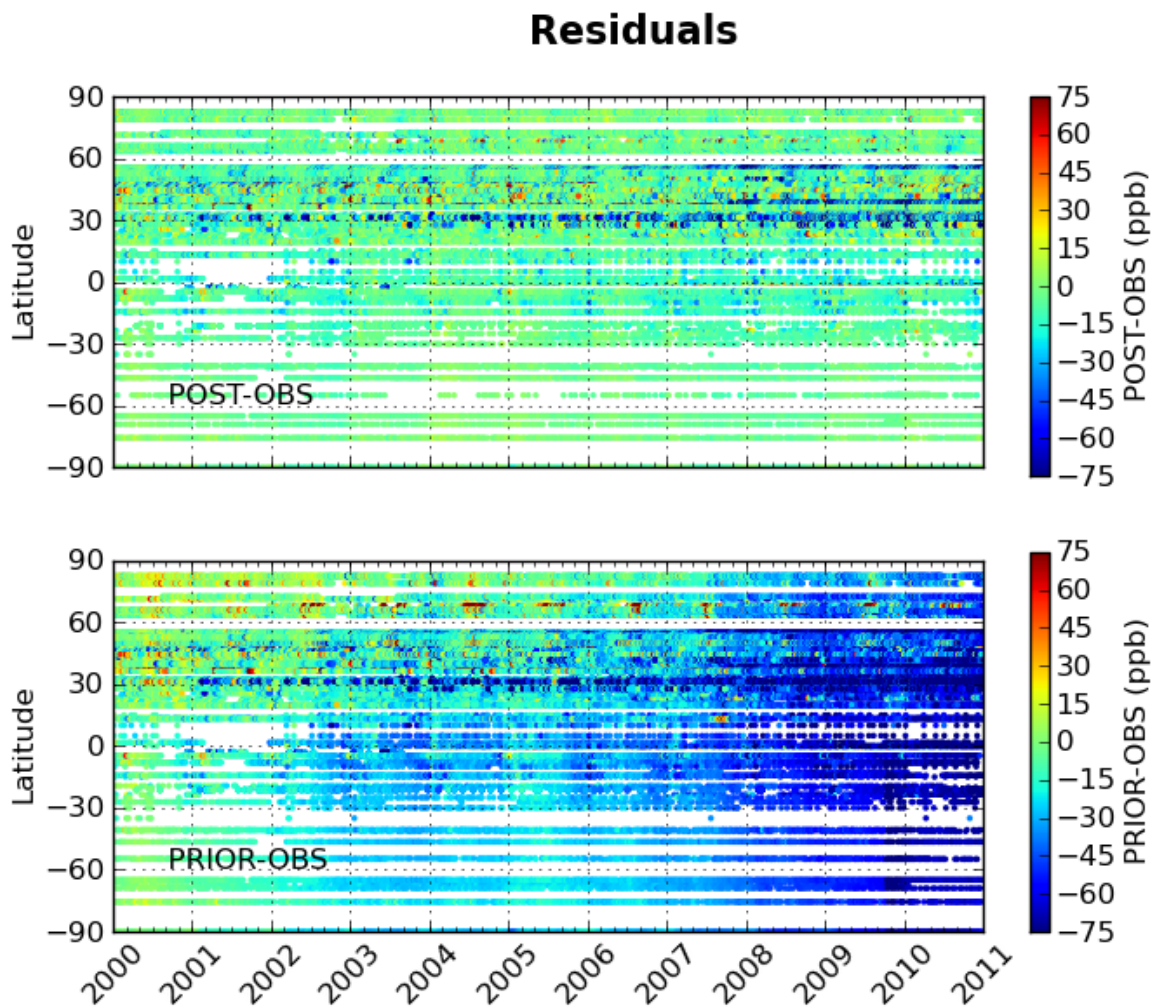
11

12

13

14

15



2

3

4

5 **Figure 2** - The CarbonTracker posterior residuals (simulated minus observed, in  
6  $\text{nmol mol}^{-1}$ ) as a function of time and latitude (top) and prior residuals (bottom). Each  
7 dot represents the time and location of a  $\text{CH}_4$  observation that was assimilated in  
8 CarbonTracker. Colors represent the difference between the final simulated value  
9 and the actual measurement, with warm colors indicating that CarbonTracker  
10 simulates too much methane compared to observations, and cool colors indicating  
11 that CarbonTracker estimates too little.

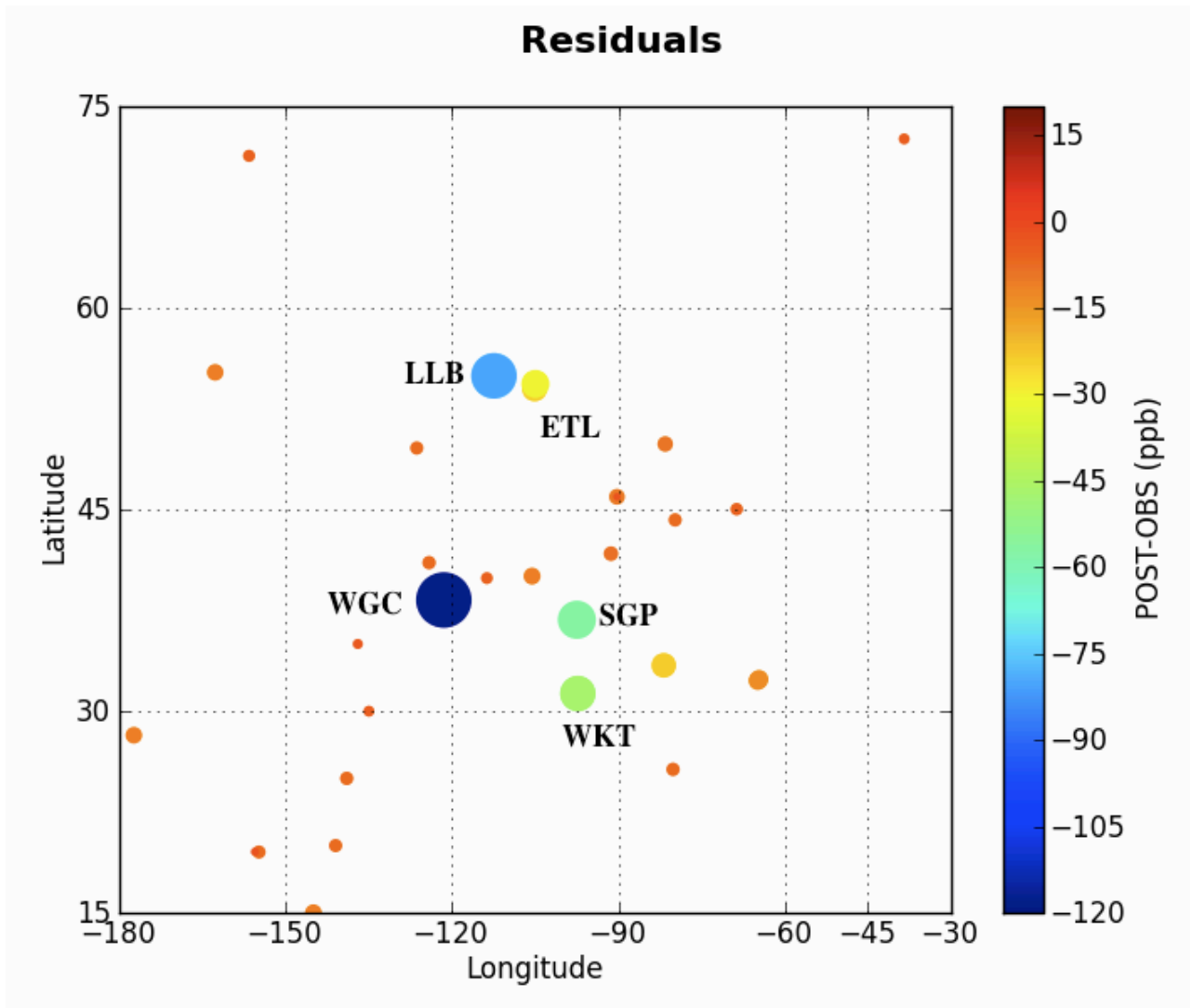
12

13



1

2



3

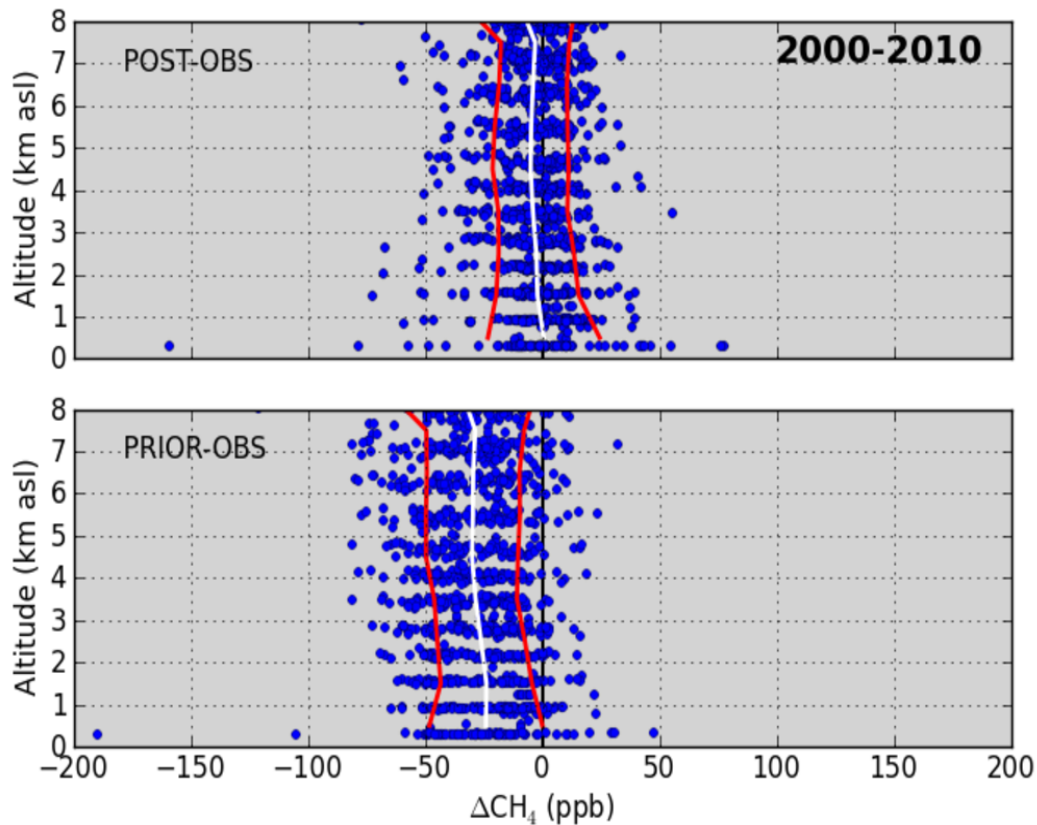
4

5 **Figure 3** - The CarbonTracker posterior residuals (simulated minus observed, in  
6 nmol mol<sup>-1</sup>) as a function of time and latitude for North America. Each bubble has a  
7 radius proportional to the size of the residual, and the values are also indicated by  
8 the color bar. The largest residuals found by CarbonTracker-CH<sub>4</sub> are labeled also by  
9 site code.

10

11

## THD\_01P2 (Not Assimilated)



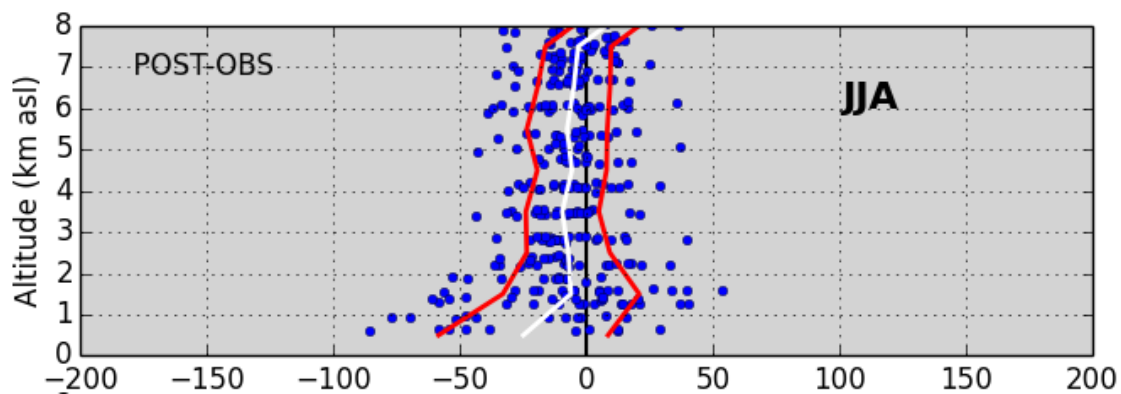
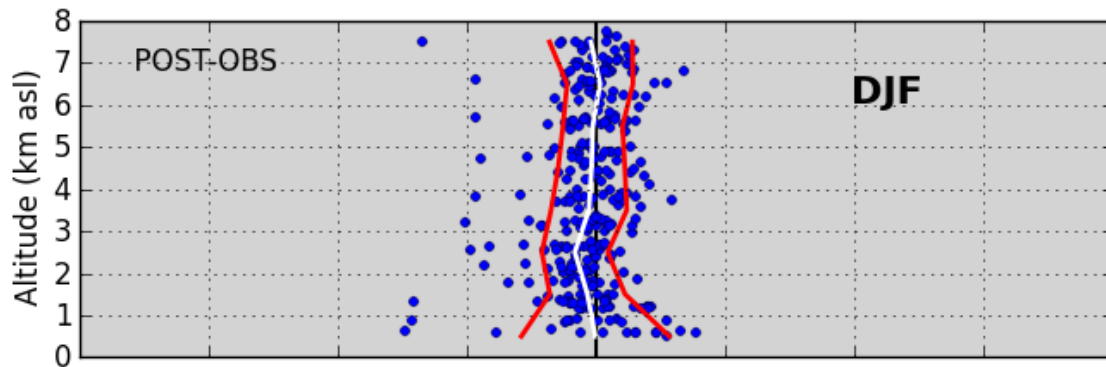
1

2 **Figure 4** - Statistical summary of residuals for aircraft profiles at a site sampling  
3 marine air (Trinidad Head, CA). Units are  $10^{-9}$  mol mol<sup>-1</sup> of CH<sub>4</sub> (ppb). The top figure  
4 shows the post-assimilation residuals (posterior-observed) and the bottom figure  
5 shows the residuals with no data assimilation (prior-observed). Aircraft data are not  
6 currently assimilated in CarbonTracker so they provide an independent evaluation of  
7 the data assimilation. Ideally, the mean of the residuals for the simulations with data  
8 assimilation should be near zero. The residuals for the simulations without data  
9 assimilation, on the other hand, tend to show large biases.

10

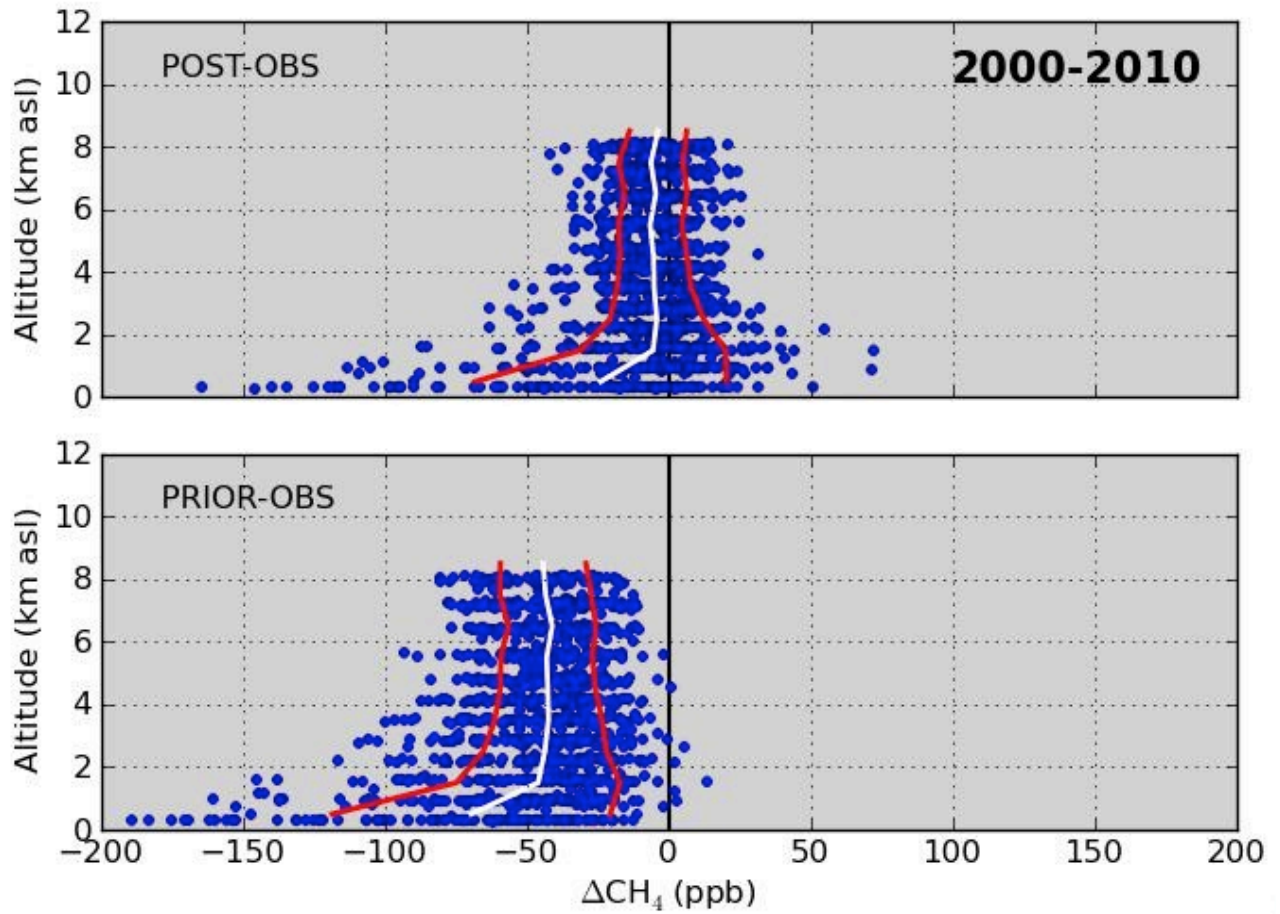
11

## DND\_01P2 (Not Assimilated)



4 **Figure 5** - Statistical summary of residuals for aircraft profiles at a site sampling  
5 continental air (Dahlen, ND; 47.5N, 99.2W). Units are  $10^{-9}$  mol mol<sup>-1</sup> of CH<sub>4</sub> (ppb).  
6 The top figure shows the post-assimilation residuals (posterior-observed) for winter  
7 months and the bottom figure shows the post-assimilation residuals for summer  
8 months. Note that summertime emissions near the surface are underestimated.  
9 Aircraft data are not currently assimilated in CarbonTracker so they provide an  
10 independent evaluation of the data assimilation. Ideally, the mean of the residuals for  
11 the simulations with data assimilation should be near zero. The residuals for the  
12 simulations without data assimilation, on the other hand, tend to show large biases.  
13

## TGC\_01P2 (Not Assimilated) (27.73N, 96.86W)



1

2

3 **Figure 6** - Statistical summary of residuals for aircraft profiles at a site sampling  
4 continental and marine air near strong local sources. Units are  $10^{-9}$  mol mol<sup>-1</sup> of CH<sub>4</sub>  
5 (ppb). The top figure shows the post-assimilation residuals (posterior-observed) for  
6 and the bottom figure shows the pre-assimilation residuals (prior-observed). The  
7 mean of the residuals for the simulations with data assimilation should be near zero.  
8 The residuals for the simulations without data assimilation, on the other hand, tend to  
9 show large biases.

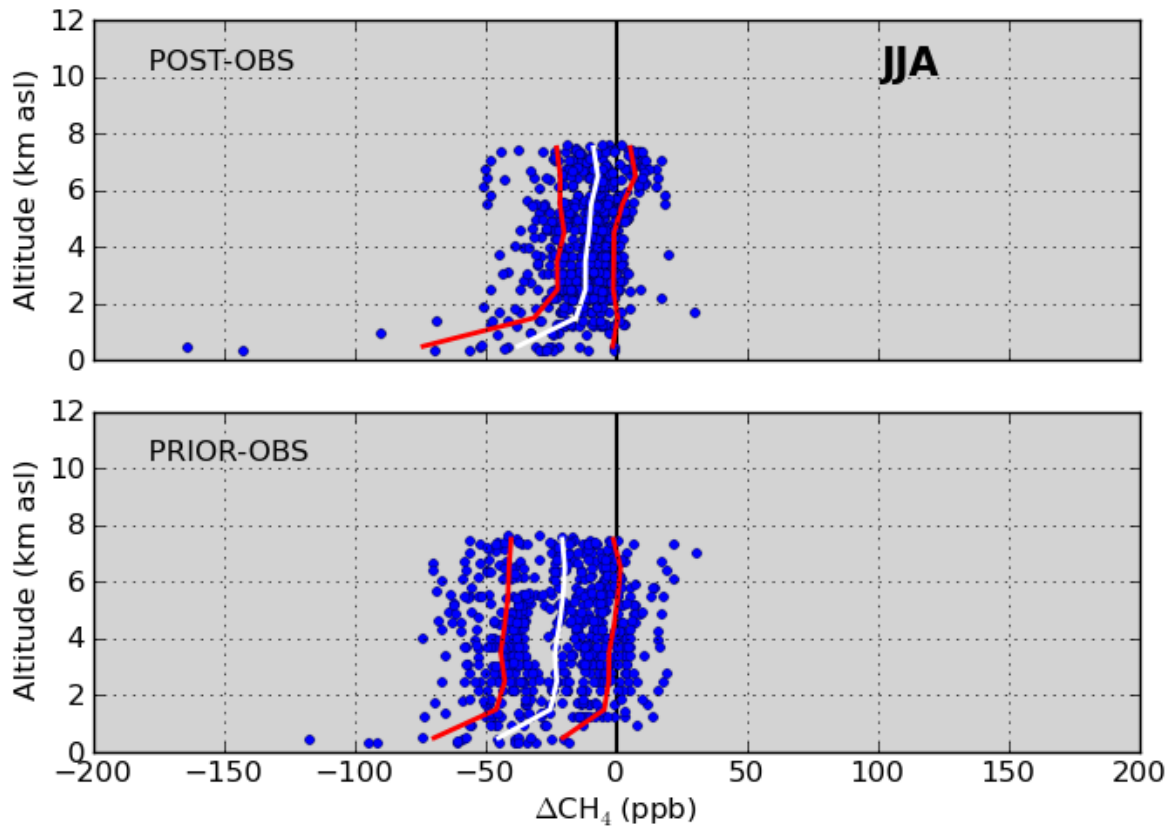
10

11

12

1

### PFA\_01P2 (Not Assimilated) (65.07N, 147.29W)



2

3 **Figure 7** - Statistical summary of residuals for aircraft profiles at a high latitude site in  
4 Alaska during boreal summer. Units are  $10^{-9}$  mol mol<sup>-1</sup> of CH<sub>4</sub> (ppb). The top figure  
5 shows the post-assimilation residuals (posterior-observed) for and the bottom figure  
6 shows the pre-assimilation residuals (prior-observed). The mean of the residuals for  
7 the simulations with data assimilation should be near zero. The residuals for the  
8 simulations without data assimilation, on the other hand, tend to show large biases.

9

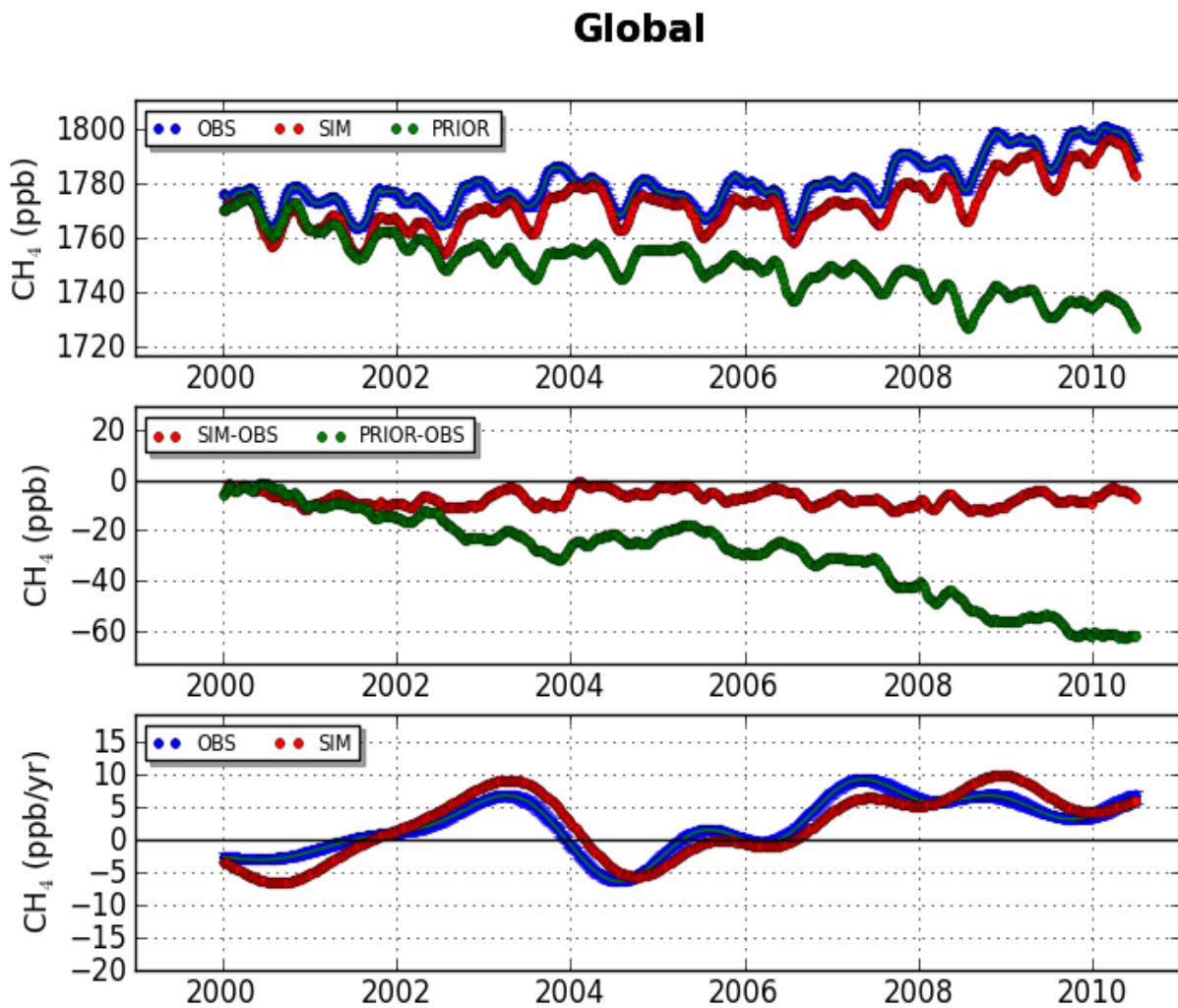
10

11

12

13

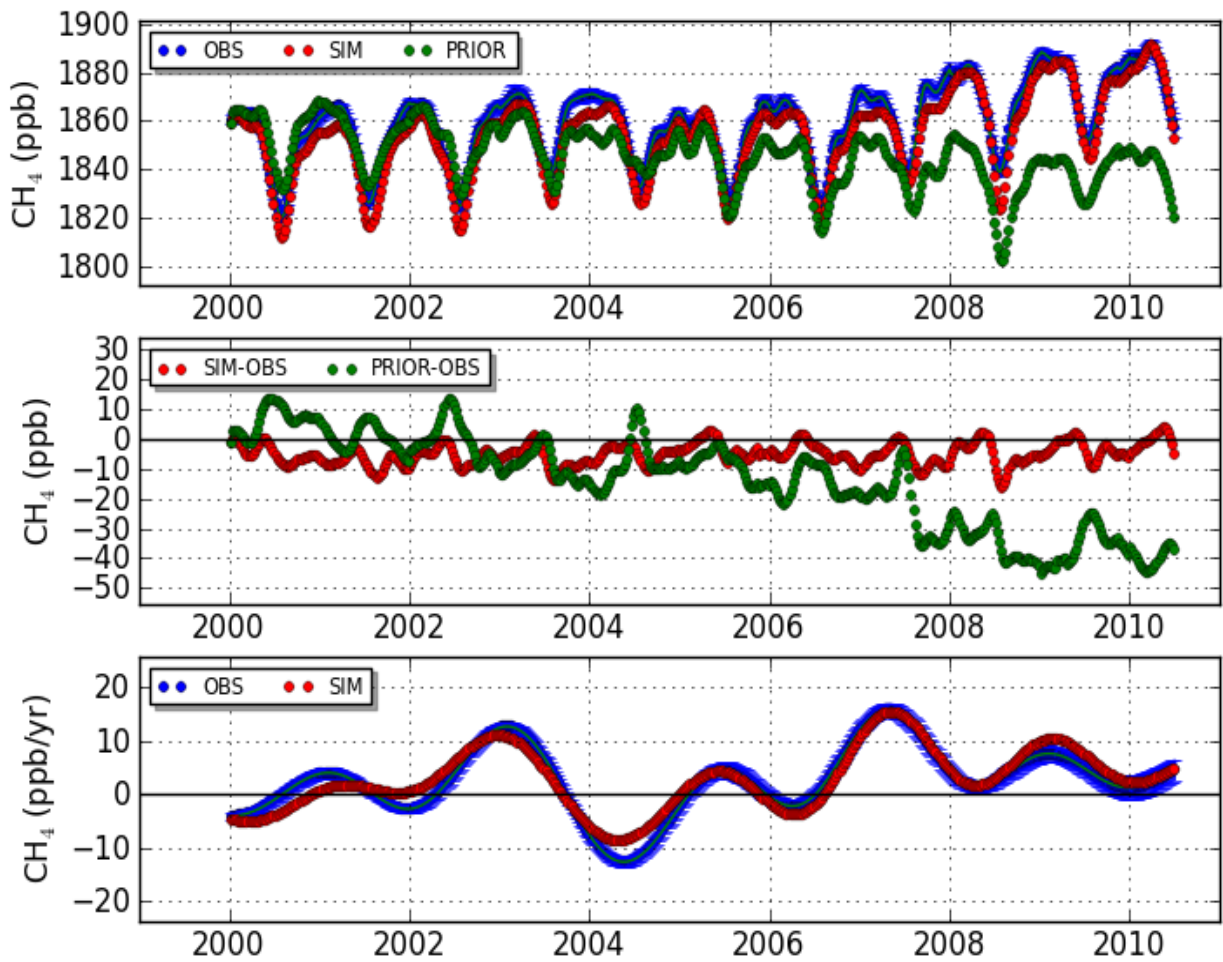
14



2

3 **Figure 8** - (Top) De-seasonalized time series of observed (dark blue, "OBS", with  
 4 very small error bars estimated using a bootstrap technique), assimilated (red, "SIM")  
 5 and prior (green, "PRIOR") average methane mole fraction. For the "PRIOR"  
 6 simulations, prior fluxes were used to calculate CH<sub>4</sub> mole fractions, while for the  
 7 "SIM" simulations CH<sub>4</sub> was calculated using fluxes that were adjusted for optimal  
 8 agreement with atmospheric observations. Units are ppb ( $10^{-9}$  mol mol<sup>-1</sup>). (Middle)  
 9 The differences from observations for assimilated and prior CH<sub>4</sub> (ppb). (Bottom)  
 10 Derived growth rate of CH<sub>4</sub> mole fraction for observed (with error bars) and  
 11 assimilated CH<sub>4</sub> mole fraction. The growth rate is computed by taking the first  
 12 derivative of the average mole fractions shown in the top figure. Units are ppb yr<sup>-1</sup>  
 13 ( $10^{-9}$  mol mol<sup>-1</sup> yr<sup>-1</sup>).

## Polar Northern Hemisphere



1

2 **Figure 9:** (Top) De-seasonalized time series of observed (dark blue, "OBS" with error  
3 bars), assimilated (red, "SIM") and prior (green, "PRIOR") average methane mole  
4 fraction for the Polar Northern Hemisphere (53N-90N). (Middle) Differences from  
5 observations for assimilated and prior CH<sub>4</sub> (ppb). (Bottom) Derived growth rate of  
6 CH<sub>4</sub> mole fraction for observed and assimilated CH<sub>4</sub> mole fraction for the Polar  
7 Northern Hemisphere.

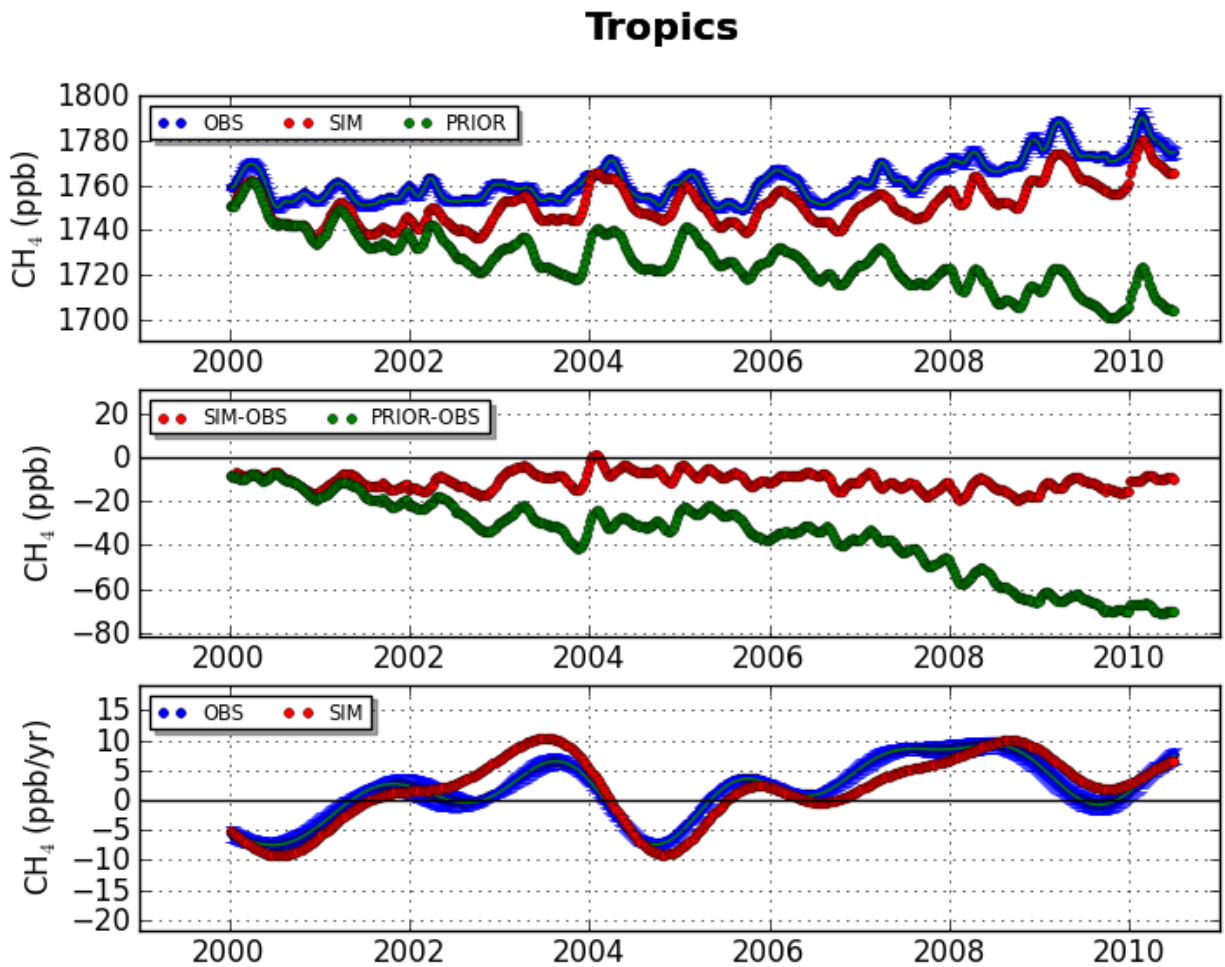
8

9

10

11

12



1

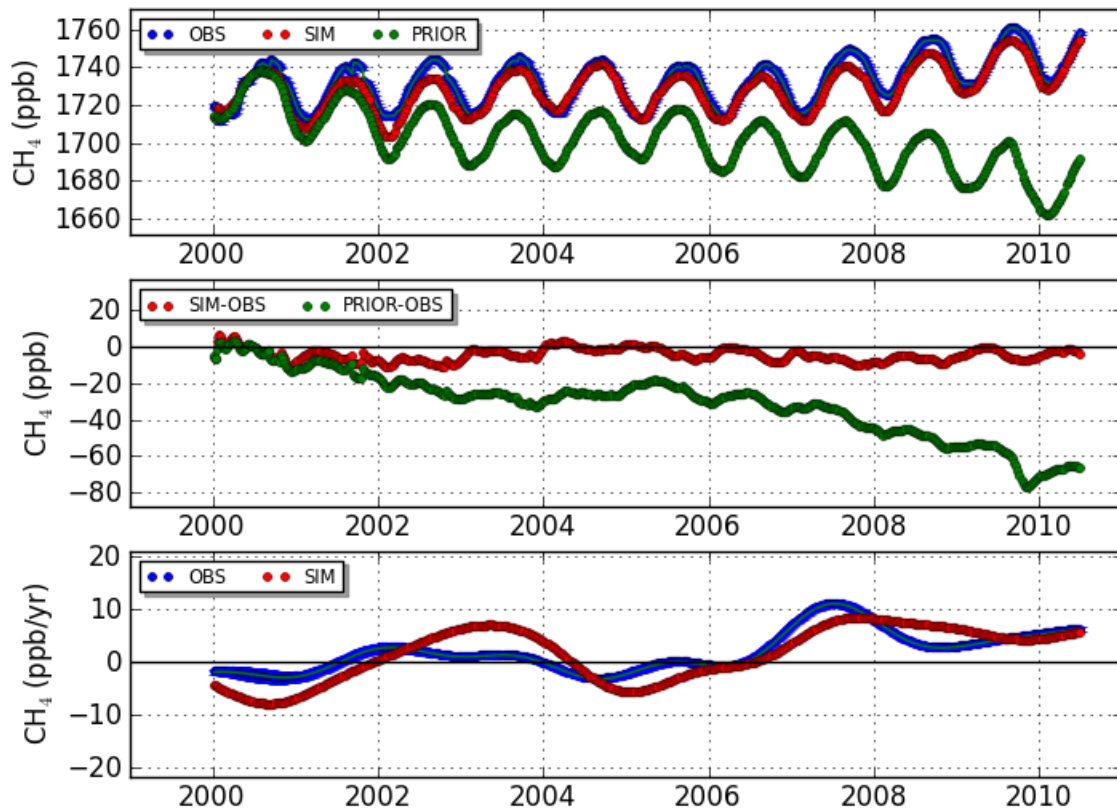
2 **Figure 10:** (Top) Time series of observed (dark blue, "OBS"), assimilated (red,  
 3 "SIM") and prior (green, "PRIOR") average methane mole fraction for the Tropics  
 4 (17.5S-17.5N). (Middle) Differences from observations for assimilated and prior CH<sub>4</sub>  
 5 (ppb). (Bottom) Derived growth rate of CH<sub>4</sub> mole fraction for observed (with error  
 6 bars) and assimilated CH<sub>4</sub> mole fraction for the Tropics.

7

8

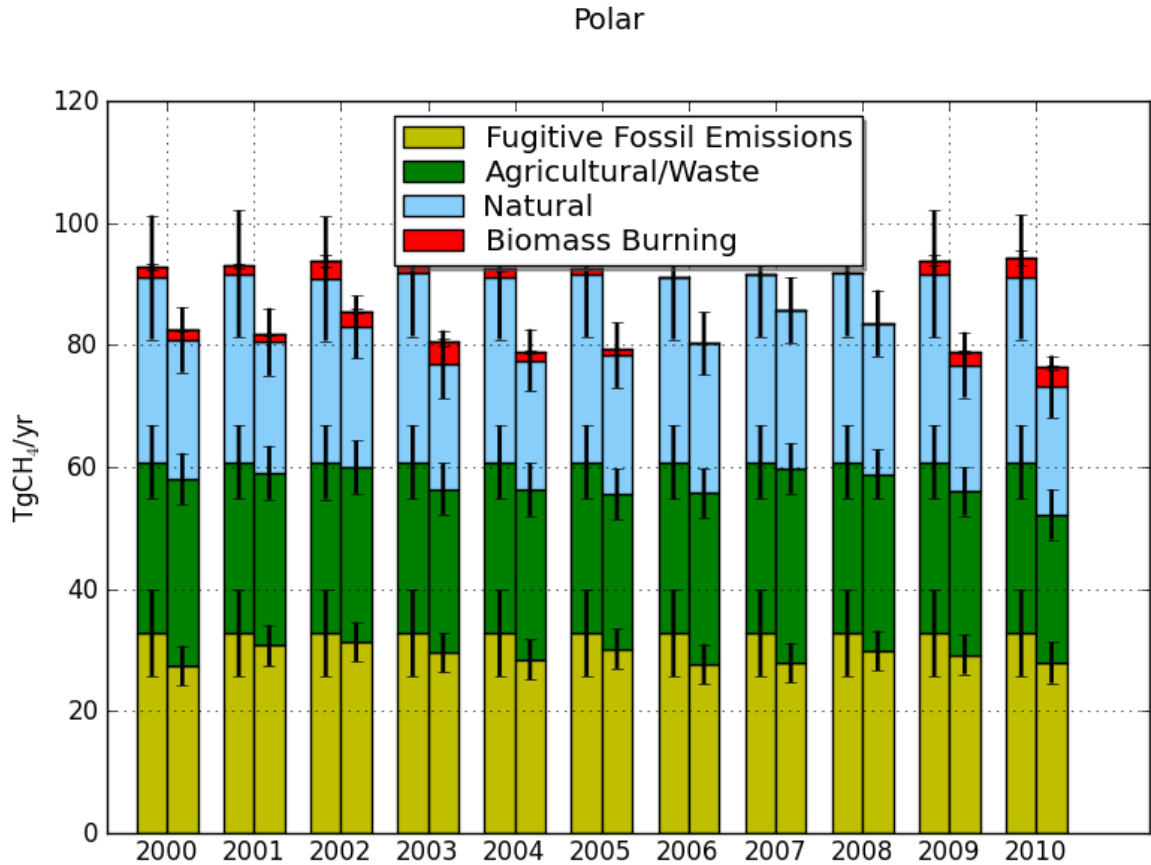


## Temperate Southern Hemisphere



1  
2  
3  
4  
5  
6  
7  
8  
9  
10

**Figure 11:** (Top) Time series of observed (dark blue, "OBS"), assimilated (red, "SIM") and prior (green, "PRIOR") average methane mole fraction for the Temperate Southern Hemisphere (17.5S-53.3S). (Middle) Differences from observations for assimilated and prior CH<sub>4</sub> (ppb). (Bottom) Derived growth rate of CH<sub>4</sub> mole fraction for observed (with error bars) and assimilated CH<sub>4</sub> mole fraction for the Tropics.



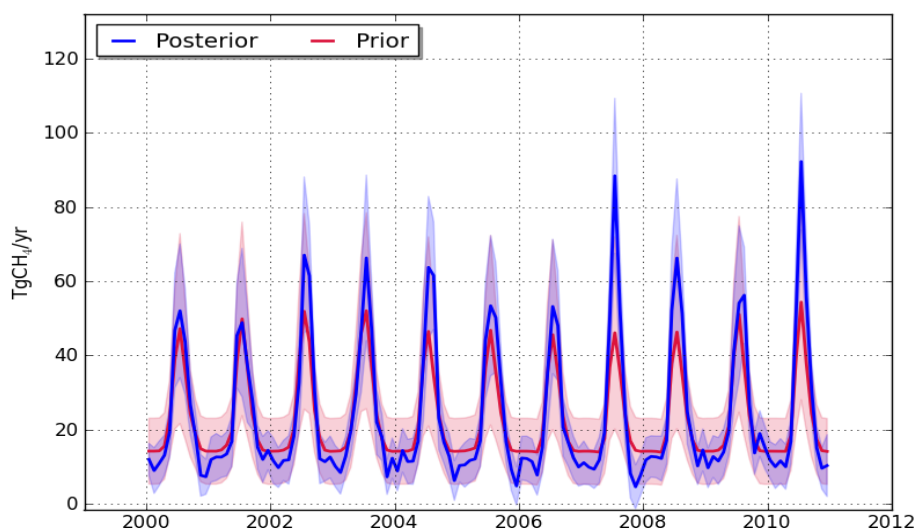
1

2 **Figure 12** - The contribution to the High Northern Latitude total CH<sub>4</sub> flux from each  
 3 category of emissions with 1- $\sigma$  error estimates. For each pair of histogram bars, the  
 4 prior flux estimates are shown on the left and the posterior estimates on the right.  
 5 Note that, except for emissions from fires, the prior flux estimates are constant for  
 6 each year. The units are Tg CH<sub>4</sub> yr<sup>-1</sup>. The average estimated uncertainty on the total  
 7 emissions is 7.5 Tg CH<sub>4</sub> yr<sup>-1</sup>.

8

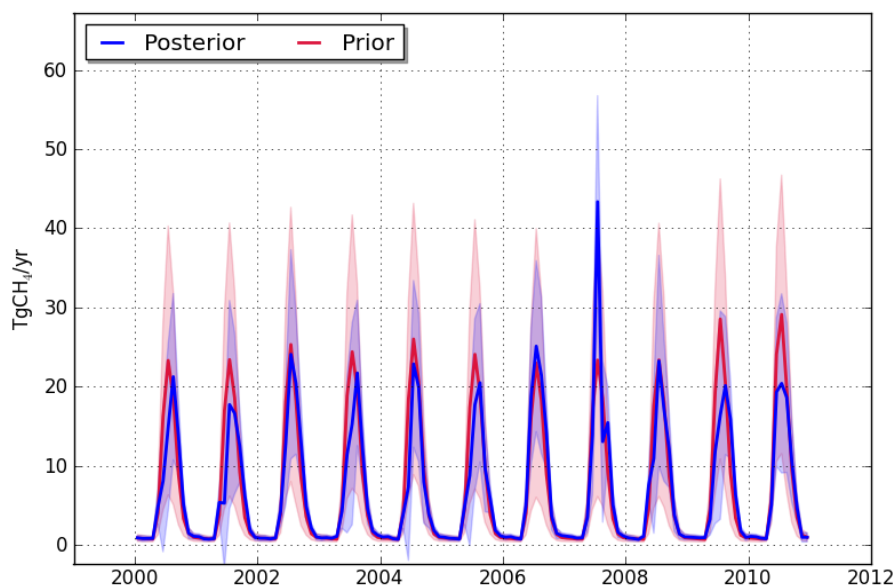
9

**Total**  
Boreal Eurasia



1

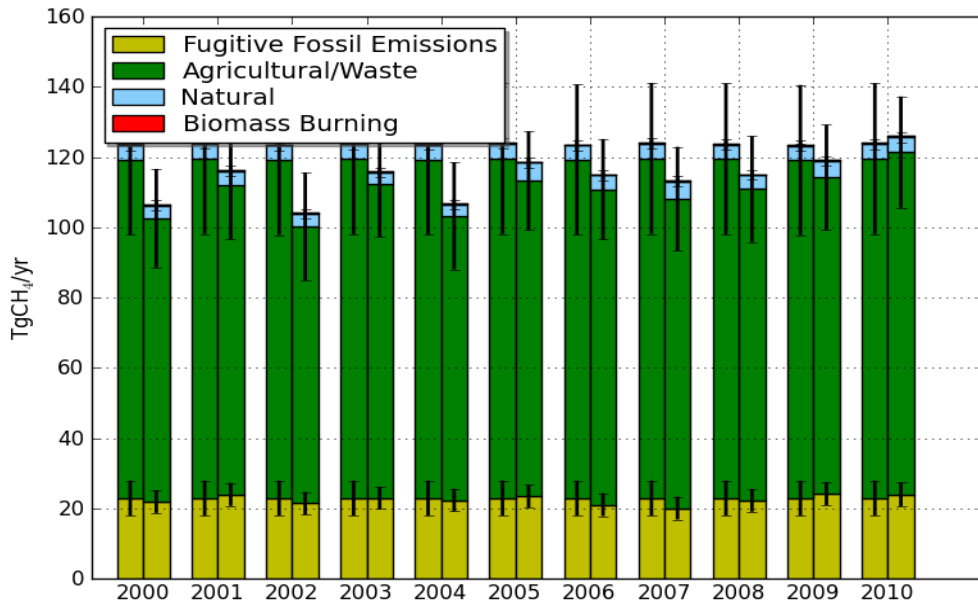
**Total**  
Boreal North America



2

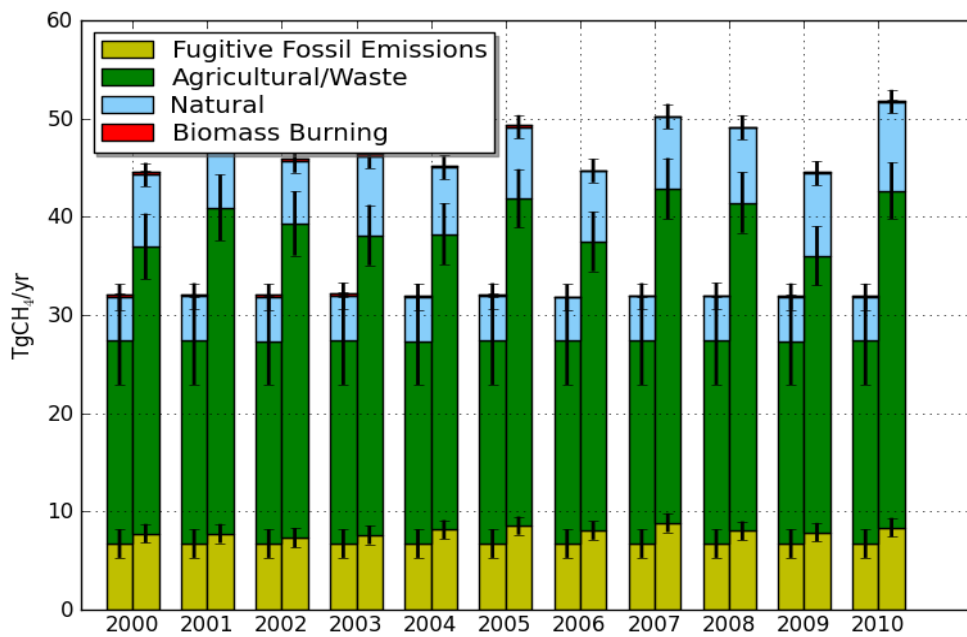
3 **Figure 13** – Time variation of the prior and estimated CH<sub>4</sub> emissions. Prior estimates  
4 are shown in red, and posterior flux estimates are shown in blue. Note that only the  
5 biomass burning prior emission estimates vary from year to year; other prior  
6 estimates are constant. 1 $\sigma$  uncertainty bounds are shown as light red (prior) and light  
7 blue (post-assimilation) shaded areas. Note that microbial sources of methane, such  
8 as wetlands and agriculture, are temperature-sensitive and therefore tend to be  
9 largest during summer. Units are Tg CH<sub>4</sub> yr<sup>-1</sup>.

Temperate Eurasia



1

Temperate North America

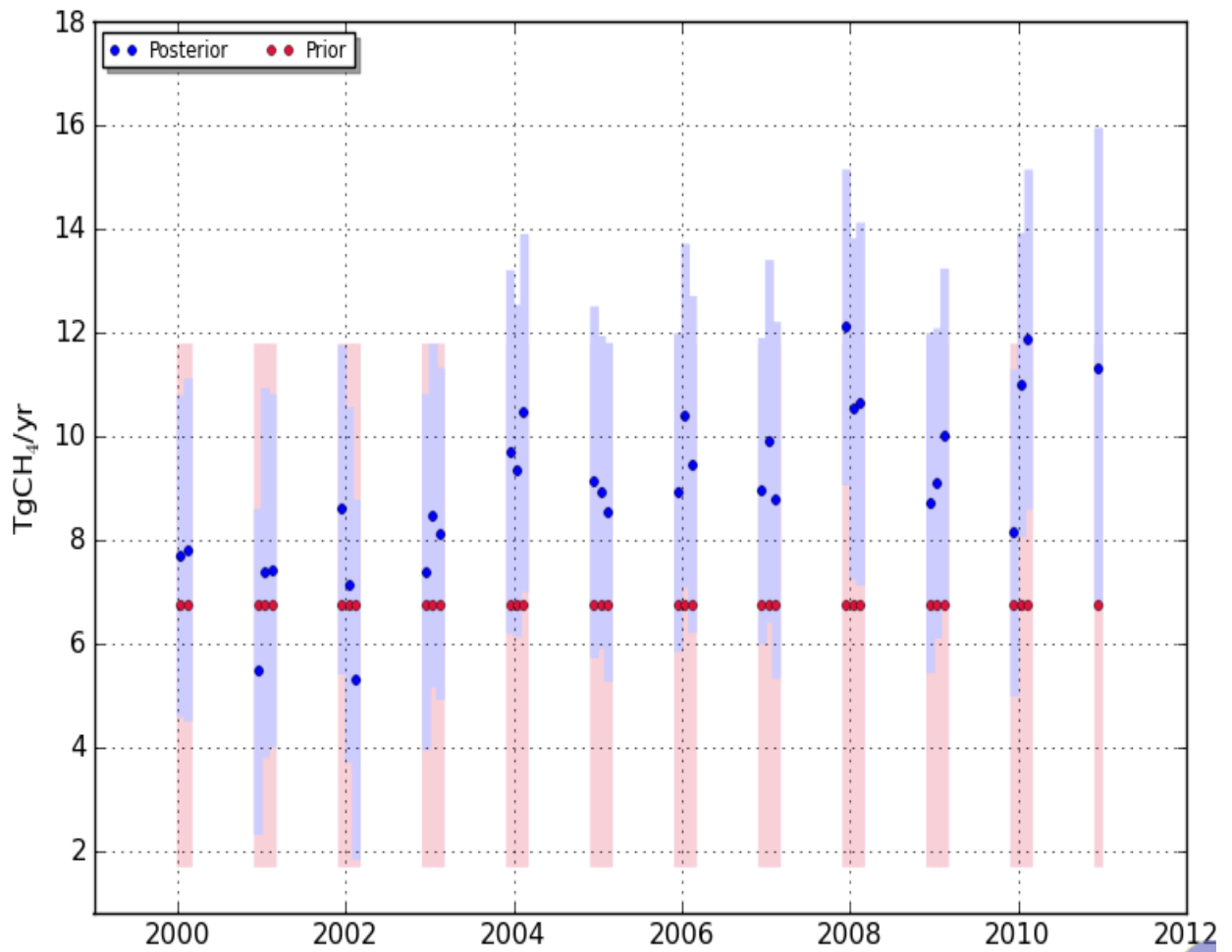


2

3 **Figure 14** - The contribution to the total CH<sub>4</sub> flux from each category of emissions  
 4 with 1- $\sigma$  error bars for Temperate Eurasia (*top*) and Temperate North America  
 5 (*bottom*). Prior flux estimates are on the left and posterior estimates on the right for  
 6 each set pair of bars. Note that, except for emissions from fires, the prior flux  
 7 estimates are constant for each year. Units are Tg CH<sub>4</sub> yr<sup>-1</sup>. The total 1- $\sigma$  errors for  
 8 all emission categories are 15.3 Tg CH<sub>4</sub> yr<sup>-1</sup> and 3.5 Tg CH<sub>4</sub> yr<sup>-1</sup> for Temperate  
 9 Eurasia and Temperate North America respectively.

# Fossil Fuel

## Temperate North America, DJF



1

2

3

4

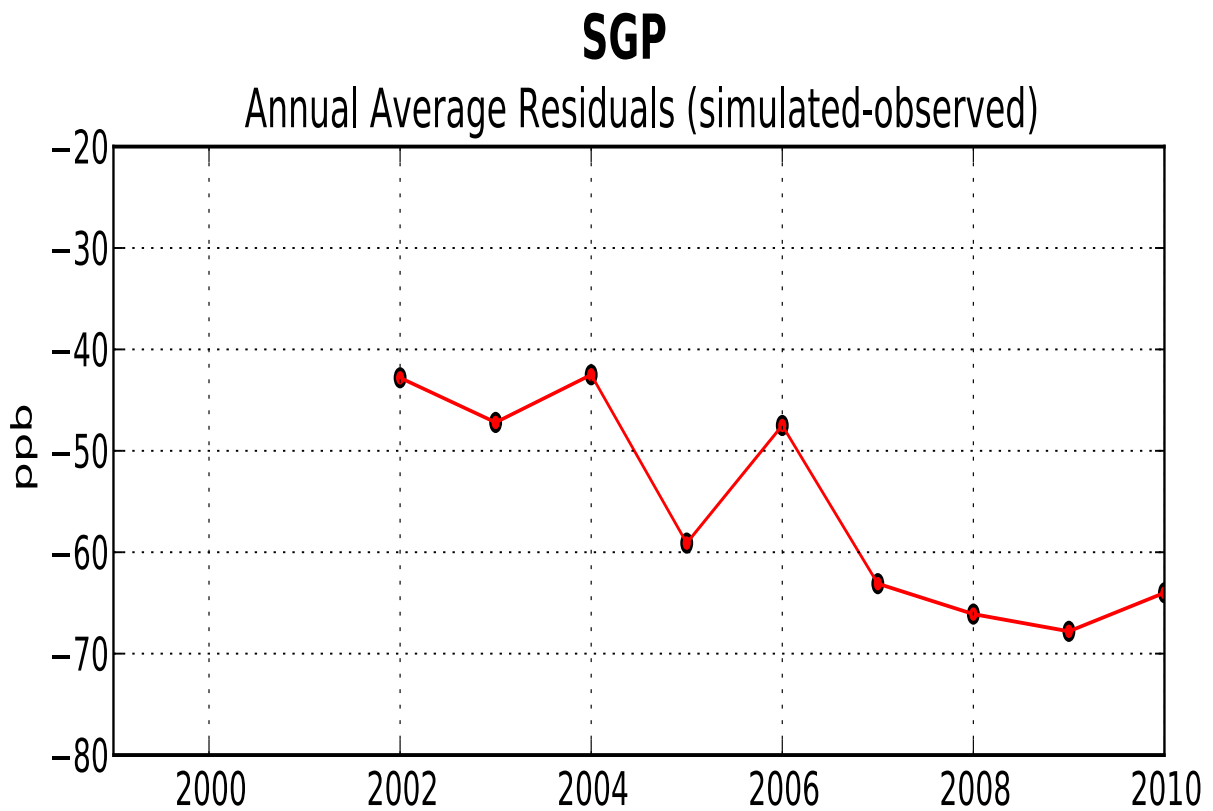
5

6 **Figure 15** - Time variation of the estimated CH<sub>4</sub> emissions from Temperate North  
7 America for winter. Prior flux estimates are shown in red, and posterior flux estimates  
8 are shown in blue. 1-σ uncertainty bounds are shown as light red (prior) and light  
9 blue (posterior) shaded areas. Units are Tg CH<sub>4</sub> yr<sup>-1</sup>.

10

11

1



2

3

4

5 **Figure 16** - Time series of residuals (the difference between the posterior and  
6 measured mole fractions). Note that the prior is constant over the length of the  
7 inversion, and the trend in the residuals can be interpreted to mean that it is  
8 increasingly difficult to fit this site over time. Units are  $10^{-9}$  mol mol<sup>-1</sup> of CH<sub>4</sub> (ppb).

9

10

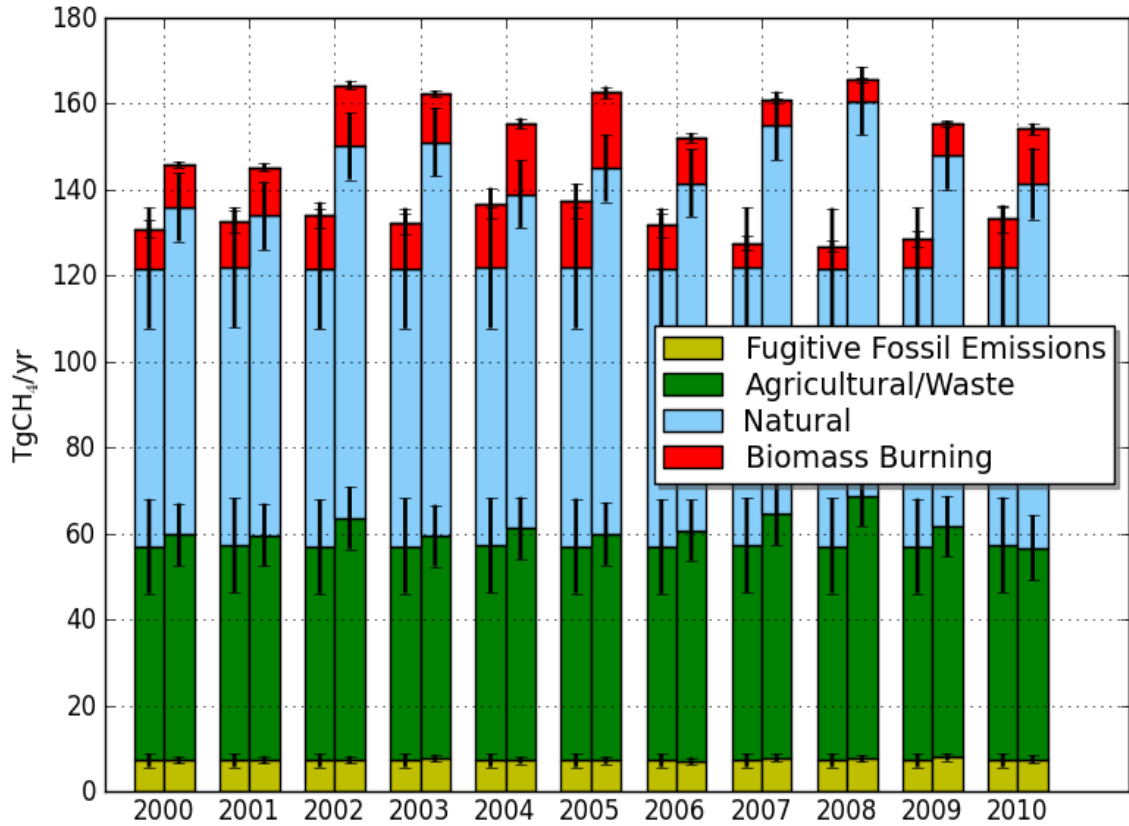
11

12

13

14

## Tropical



1

2

3

4 **Figure 17** - The contribution to the total CH<sub>4</sub> flux from each category of emissions

5 with 1-σ error bars for the Tropics (Tropical South America, Tropical Asia and

6 Tropical Africa). For each pair of histogram bars, the prior flux estimates are shown

7 on the left and the posterior estimates on the right. Note that, except for emissions

8 from fires that are very small for these regions, the prior flux estimates are constant

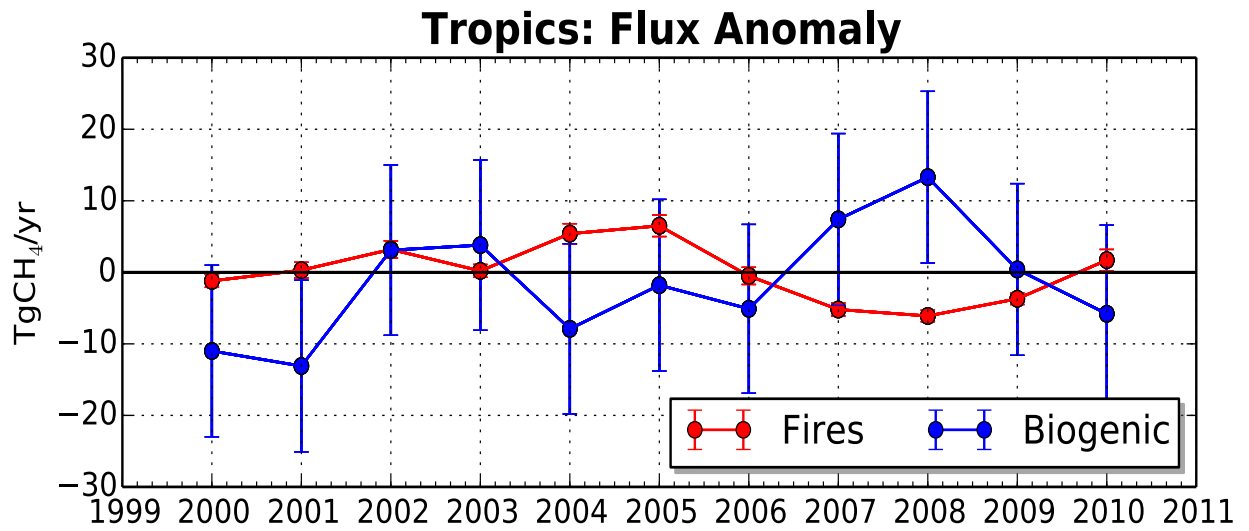
9 for each year. The units are Tg CH<sub>4</sub> yr<sup>-1</sup>. The average total estimated 1-σ error is

10 10.8 Tg CH<sub>4</sub> yr<sup>-1</sup>.

11

12

1  
2  
3



4  
5  
6  
7  
8  
9  
10  
11  
12

**Figure 18** - Time variation of estimated total biogenic (wetlands and agriculture/waste) and fire CH<sub>4</sub> emission anomalies. Anomalies are calculated with respect to 10-year average posterior emissions. The units are Tg CH<sub>4</sub> yr<sup>-1</sup>. The error bars represent 1-σ estimated error bounds on the flux anomalies.